Exploring Organic-mineral Evolution in Planetary Analogs: Insights from Hydrothermal Alteration of Aromatic Molecules and Mafic Minerals

Vassilissa Vinogradoff, Vincent Chevrier, Olivier Grauby, Marie-Vanessa Coulet, Florence Chaspoul, John Carter

The Planetary Science Journal, 6:189 (30pp), 2025 August https://doi.org/10.3847/PSJ/adf1e4

Exploring Organic-mineral Evolution in Planetary Analogs: Insights from Hydrothermal Alteration of Aromatic Molecules and Mafic Minerals

Vassilissa Vinogradoff[1], Vincent Chevrier[2], Olivier Grauby[3], Marie-Vanessa Coulet[4], Florence Chaspoul[5], and John Carter[6]
[1] Aix-Marseille University, CNRS, PIIM—UMR 7345, Marseille, France; vassilissa.vinogradoff@univ-amu.fr
[2] Arkansas Center for Space and Planetary Sciences, Department of Geosciences, University of Arkansas, Fayetteville, AR 72701, USA
[3] Aix-Marseille University, CNRS, CINAM, UMR 7325, Marseille, France
[4] Aix-Marseille University, CNRS, MADIREL—UMR 7246, Marseille, France
[5] Institut IMBE-UMR 7263, CNRS, Aix-Marseille University, IRD-UMR 237, Avignon University, Marseille, France
[6] University Paris-Saclay, CNRS, IAS UMR 8617, Orsay and Aix-Marseille University, LAM UMR-CNRS 7326, Marseille, France
Received 2024 December 20; revised 2025 July 11; accepted 2025 July 15; published 2025 August 13

Abstract

Organic-mineral interactions are crucial drivers of diversity in abiotic systems on planetary surfaces. Despite their significance, the evolution of these systems, particularly the role of organic molecules in newly formed minerals, remains underexplored. In this study, we proposed new experiments on analogs to explore the interactions between organic molecules likely present in planetary environments and primary minerals. We examine interactions between aromatic benzyl-group compounds and igneous minerals (olivine, feldspar) under mid-temperature aqueous conditions, analogous to hydrothermal systems hypothesized to exist on early Martian and terrestrial environments. Using multiscale techniques—gas chromatography, infrared spectroscopy, mass spectrometry, X-ray diffraction, microscopy, and adsorption studies—we analyzed the analogs after 45 days at 100°C. The results reveal that the presence of minerals influences the distribution of newly formed organic compounds, for example, by promoting the formation of organic chelates. Minerals altered in the presence of organics formed secondary phases, such as phyllosilicates and amorphous materials resembling serpentines or smectites. Organic compounds impacted dissolution rates, secondary mineral parageneses, and porosity, enriching the diversity of hydrated mineral phases compared to mineral alteration without organic matter. Significant carbon and nitrogen were found filling mineral porosity (up to 7 wt% C), modifying physical properties compared to systems without organics. These findings highlight the pivotal role of organics in shaping mineralogy on planetary surfaces and underscore the need for broader studies of organic-mineral analogs to improve interpretations of in situ and remote organic detections in extraterrestrial samples.

Unified Astronomy Thesaurus concepts: Astrochemistry (75); Complex organic molecules (2256); Planetary mineralogy (2304); Cosmochemistry (331)

1. Introduction

One of the key questions in planetary science is how the (co) evolution between the mineralogical and chemical realms can affect the chemical and physical properties of each phase and alter their signatures and chemical analysis (M. Schoonen et al. 2004; J. Ganor et al. 2009; H. J. Cleaves et al. 2012). In particular, water is a key driver of the interaction between abiotic organic matter and primary minerals in many bedrock and hydrothermal environments (aqueous medium with temperatures typically above 50°C) and can increase diversity and complexity. The expected decomposition, transformation, or adsorption of organic molecules mixed with minerals during hydrothermal alteration that we particularly consider here, have major implications for their detection and observation today at the surface of planets or moons. Hydrothermal weathering of rocks is a common process that has occurred or still occurs in astrophysical environments capable of sustaining liquid water. Mars was one of these aqueous environments billions of years ago, in the context of seafloor or lake-bottom hydrothermal systems and we find traces of these processes today (A. Gaudin et al. 2011; N. Mangold et al. 2012; J. R. Michalski et al. 2017). Today, Mars is partially covered by phyllosilicates and other hydrated minerals, attesting to aqueous alteration about 3–4 billion years ago (L. Riu et al. 2019; J. Carter et al. 2013, 2023). It is particularly in such past hydrous environments that organic matter is being sought (J. L. Eigenbrode et al. 2018; M. Millan et al. 2022; S. Sharma et al. 2023). On Earth, the diversity and complexity of mineral-organic systems formed by hydrothermal weathering in soils or sediments (L. M. Mayer 1994; M. Kleber et al. 2015; J. D. Hemingway et al. 2019) suggest a huge potential of such interactions for abiotic extraterrestrial systems. Geological hydrothermal systems, akin to hydrothermal vents on Earth, accumulate organic and inorganic materials whose molecular distribution varies with temperature and pressure conditions, which remain poorly understood (A. D. Aubrey et al. 2009; M. Colín-García et al. 2016; H. Xu et al. 2024). However, because life plays a major role in such systems on Earth, we cannot extrapolate Earth mineral-organic interactions to solar system bodies. In addition to the study of natural analogs from Earth-based hydrothermal systems (reviews and reference therein: J. J. Marlow et al. 2011; F. Foucher et al. 2021; B. L. Teece et al. 2024), experimental studies of abiotic matter and primary minerals are essential to establish constraints for understanding other extraterrestrial environments such as Mars, as well as the early Earth before life. These studies are crucial for detecting and identifying organic molecules (OM) within mineral matrices, uncovering

their true history, and distinguishing abiotic signatures from potential biosignatures.

In the context of extraterrestrial planetary environments, organic-mineral interactions have raised interest in the perspective of biomineralization and biogenic minerals for biosignatures decoding (see, for example, M. A. Chan et al. 2019; S. McMahon & J. Cosmidis 2022 and references therein). These organic-mineral processes resulting from hydrothermal alteration have, to a lesser extent because of water abundance, occurred on small bodies of our solar system, as shown in the studies of carbonaceous chondrites and dwarf planet Ceres (see, for exemple, C. Le Guillou et al. 2014; J. C. Castillo-Rogez et al. 2018; Y. Kebukawa et al. 2019). Mineral-organic interactions in hydrothermal environments are often proposed as a key process in prebiotic chemistry (M. Schoonen et al. 2004; J. R. Brucato & T. Fornaro 2019), and could have indeed boosted new chemical pathways toward the emergence of a prebiotic chemistry (H. J. Cleaves et al. 2012; M. Colín-García et al. 2016; K. B. Muchowska et al. 2019; C. Lee et al. 2022; V. Vinogradoff et al. 2024; T. J. de Jong et al. 2025). In addition, some minerals can protect the organic molecules from further degradation (e.g., hydrolysis, surface irradiation, or oxidation, for example) and are therefore an invaluable asset for their preservation (L. M. Mayer 1994; O. Poch et al. 2015; R. dos Santos et al. 2016; G. Ertem et al. 2017; J. D. Hemingway et al. 2019). Many studies have postulated the potential of minerals for preservation of organic molecules, especially phyllosilicates, because they can adsorb organic molecules within their sheets. However, this preservation potential is highly dependent on the phyllosilicates compositions, or the nature of the organic molecules since absorption depends on many parameters, such as the ph, the charges of the minerals, the presence of Lewis or Bronsted sites, or the hydrogen bonds of the molecules (see reviews by G. Lagaly et al. 2013; M. Kleber et al. 2021). In addition, an aspect of organic-mineral interactions that has received little attention is the effect of organic molecules on the secondary paragenesis of mafic minerals. Organic molecules, because of their intrinsic properties can indeed play a role of catalyst, modify the dissolution of minerals or their structure, and or prevent the crystallization of the mineral (M. Kleber et al. 2015; P. Jacquemot et al. 2019). In this study, we hypothesize that the nature of abiotic organic molecules influences the transformation of mafic minerals during simulated hydrothermal alteration within a simplified planetary context. Additionally, we propose that organic-mineral interactions constitute a key process shaping the evolution of both organic and mineral phases and the preservation potential.

We conducted a case study examining the interaction of primary minerals with abiotic organic molecules in a hydrothermal setting (close to a surface hydrothermal vent) to understand alterations in both phases and produce relevant analogs. Nonhydrated primary silicates were mixed with functionalized aromatic and aliphatic molecules and reacted for 45 days at 100°C under anoxic conditions. The extended duration is intended to provide adequate time for the system to react within the laboratory's allocated timeframe, thereby enabling observation of the interaction. The medium temperature selected for the hydrothermal system is intended to facilitate the retention of the majority of water in its liquid phase, thereby ensuring optimal reactivity.

Magnesium-rich olivine (O) and sodium-rich plagioclase (F), common in mafic rocks on Earth and early Mars, were used as model minerals, with phyllosilicates expected as primary alteration products. Organic molecules were chosen to represent types detected or suspected on Mars: benzoic acid (Bz, acidic), toluene (T, neutral), benzylamine (By, alkaline), and propanol (Pr, alcohol-functionalized alkane; C. Freissinet et al. 2015; J. L. Eigenbrode et al. 2018; M. Millan et al. 2021, 2022). Additional experiments included minerals alone or with potassium hydroxide (KOH) to assess pH effects. Products were characterized using multiple techniques to ensure a complete characterization of the samples: gas chromatography–mass spectrometry (GC-MS), infrared spectroscopy (FTIR), mass spectrometry (ICP-MS), X-ray diffraction (XRD), electronic microscopy (TEM, SEM), gas-adsorption techniques (BET), and elemental composition (EA).

2. Methods

2.1. Experimental Protocol

2.1.1. Mineral Powders

The Mg-rich olivine (namely peridot) was obtained from San Carlos, Arizona. The formula of our olivine sample (measured in this study by TEM-EDX, Figure A5) was $Mg_{1.9}Fe_{0.1}SiO_4$. Na-rich plagioclase Feldspar was selected and acquired from Minerals Unlimited (labeled as variety "Sunstone" from Madras, India). The approximate formula of our sample (measured in this study by electronic microscopy (TEM-EDX) is $Na_{0.8}Ca_{0.2}Al_{1.2}Si_{2.8}O_8$, so very close to the albite pole. Both initial mineral samples were ascertained to be visually pure prior to chipping off centimeter- to millimeter-sized grains. These centimeter-size grains were washed with solvents (water, dichloromethane, and methanol, 1 ml, three times each) to remove organic contamination from sample handling or biological matter and then the grains were let to dry overnight in an oven at 60°C. The minerals were then crushed mechanically in a Specamill pebble mill with agate cells to obtain a size fraction $<10\ \mu$m in order to maximize their surface reactivity with water. The fine powder was then washed again with organic solvents (dichloromethane/methanol in 1:1 vol. with sonication) to reduce again carbon contaminations, and dried at 60°C for 48 hr. The powders were not sieved, but the size distribution was estimated by transmission and scanning electron microscopy (TEM and SEM) observations (see Figure A5).

2.1.2. Sample Preparation

Organic compounds, benzylamine, benzoic acid, toluene, propanol (all with a purity >99.5%), and other referenced molecules were purchased from Sigma–Aldrich. The quartz cells and the Teflon reactors used in this study were cleaned before and in between experiments as follows: mechanically washed with water, sonicated with water x3, methanol x3, and dried in an oven at 110°C overnight. The quartz cells were in addition heated to 500°C for 4 hr after solvent cleaning. Milli-Q water was produced in the laboratory (Merck, conductivity $<18.2\ M\Omega\ cm^{-1}$), and then degassed with nitrogen before entering the glove box. All mineral–solution mixtures were prepared inside an anoxic chamber under argon atmosphere (>99.999%, Air Liquide ALPHAGAZ 1). Solutions were made in the glove box, loaded into closed quartz cells, then inserted into teflon reactors (PTFE), themselves inserted in steel reactors and made airtight under argon atmosphere (Figure 1). The steel reactors were then

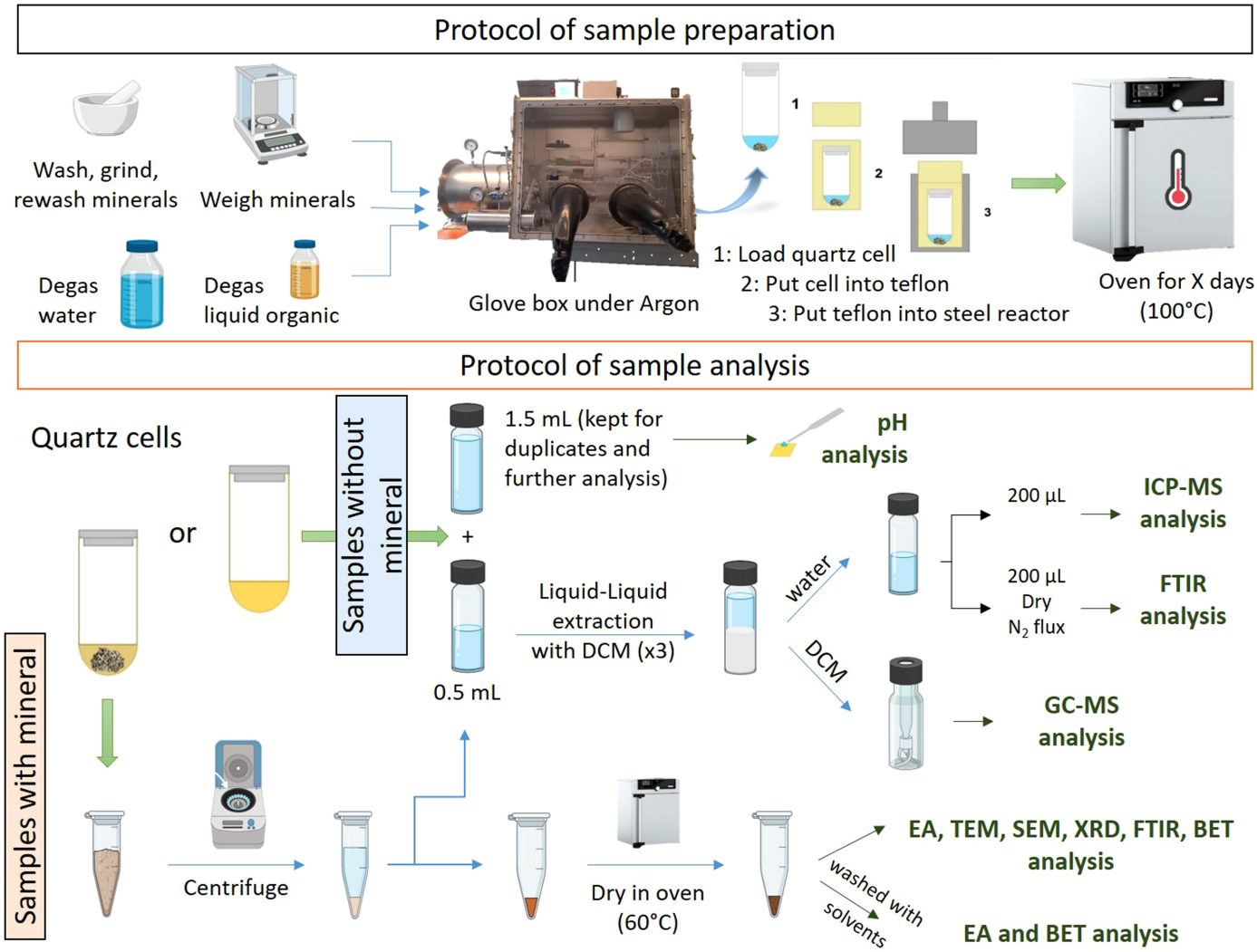

Figure 1. Detailed protocol of the sample preparation and analysis described in the method section. The samples are initially prepared by combining minerals and organic compounds within the glove box, subsequently loading them into sealed reactors prior to their transfer into the furnace. Subsequent to the completion of the experiments, an analytical protocol (detailed in the supplementary text) was applied to separate the solid from the liquid phase and/or to perform liquid–liquid extraction. The analytic techniques employed for each phase are indicated (see Section 2.2).

removed from the glove box and put in an oven for heating at 100°C for 45 days.

Organic compounds concentrations were fixed at 0.25 M each in 2 ml of water (0.5 mmol of each compound, Table 1). 100 mg of minerals were subsequently added, thus yielding a water-to-rock (W/R) ratio of 20 and an organic to mineral ratio of ∼1:1.2 in weight. The selected ratios were designed to represent a water-dominated environment, characterized by a high concentration of organic matter with minerals, with the aim of facilitating an increased level of interaction. When both minerals were mixed, the ratio of Mg-rich olivine to Na-rich feldspar was 1:3, with the same organic/mineral ratio. A larger quantity of feldspar was added to better reflect the Mars surface composition. In one solution, the organic concentration was voluntarily reduced by a factor 10 (experiment's label O +By/10+Pr/10) to test the effect of organic concentration on the result. One solution was also made with a slightly alkaline solution (in KOH, pH 8) instead of pure MilliQ water to test the effect of pH (Table 1). A water-only sample, made in the same conditions, was also done to control the level of potential contamination (no contamination was observed). For the mineral, the "blank" samples were O w/o OM and OF w/o OM (Table 1), and described as experiments in the study. Experiments involving only minerals or organic molecules alone, or the olivine series were conducted in duplicate. The outcomes of these duplicate experiments were found to be analogous, and thus, only one set of results is presented herein.

2.1.3. Sample Analysis

After completion of the reaction, samples were opened in room air and centrifuged in Eppendorf tubes (eppendorf biopur, 2 ml, 12 minute at 13,000 rpm) to separate the solid from the liquid fractions (Figure 1) and to prepare the different fractions for analysis. The detailed analytical protocol is schematized in Figure 1, and described in the supplementary material. Note that identical volumes of liquid were found after experiments in the cells, indicating that the reactors were hermetically closed.

2.2. Analytical Techniques

Elemental Analysis (EA). The hydrogen, nitrogen, and carbon contents of the solid fraction (before and after washing

Table 1
Composition of the Experimental Samples Made in This Study: the Concentration of the Organic Molecules and Quantity of Mineral for Each, Their Short Names Used in the Following Text

	Organic Concentration (mM)				Inorganic Salt (mM)	Mineral (mg)		Water (mL)	
Samples' Name	Toluene	Benzylamine	Benzoic Acid	Propanol	KOH	Mg-rich Olivine	Na-rich Feldspar		pH after 45 days of Alteration
By+Pr	…	250	…	250	…	…	…	2	8
T+Pr	250	…	…	250	…	…	…	2	6
Bz+Pr	…	…	250	250	…	…	…	2	3–4
By+T+Bz+Pr	250	250	250	250	…	…	…	2	5–6
O w/o OM[a]	…	…	…	…	…	100	…	2	8
O+By+Pr	…	250	…	250	…	100	…	2	8–9
O+T+Pr	250	…	…	250	…	100	…	2	7–8
O+Bz+Pr	0	0	250	250	…	100	…	2	6–7
O+By+T+Bz+Pr	250	250	250	250	…	100	…	2	7–8
O+By/10+Pr/10	…	25	…	25	…	100	…	2	8
O+KOH	…	…	…	…	1	100	…	2	7–8
OF w/o OM[a]	…	…	…	…	…	33	67	2	8–9
OF+By+Pr	…	250	…	250	…	33	67	2	9–10
OF+T+Pr	250	…	…	250	…	33	67	2	8
OF+Bz+Pr	…	…	250	250	…	33	67	2	6
OF+By+T+Bz+Pr	250	250	250	250	…	33	67	2	7

Note. We also reported the pH measurement of the liquid phases after 45 days of hydrothermal alteration. pH was measured using a universal indicator paper, error bar is +/−1 unit. By stands for Benzylamine, Bz for Benzoic acid, T for Toluene, Pr for Propanol, O for Mg-rich olivine, and F for Na-rich feldspar.
[a] O w/o OM or OF w/o OM means the mineral without organic matter (OM).

steps; see supplementary methods) were determined using a Thermo Finnigan EA 1112 analyzer available at the Spectropole of the *Fédération des Sciences Chimiques* in Marseille, France. Analyses were duplicated on two aliquots (∼2 mg) for each experimental sample from which the mean was calculated (Table 1). Soil samples, measured before and after the samples, were used as standards. Uncertainties on the data are ±0.2 wt% for C, ±0.02 wt% for N, and ±0.1 wt for H.

GC-MS Analysis. Dichloromethane (DCM) fractions were analyzed without a derivatization step using a Thermo Trace 1300 gas chromatograph (GC) coupled with a Thermos ISQ QD mass spectrometer (MS) operated at the PIIM laboratory (Marseille, France). The GC was equipped with a STABI-LWAX (L 60 m, internal diameter 0.32 mm, thickness 0.5 μm) capillary column (polar phase, suitable for semivolatile, hydrocarbon and benzyl compounds) using helium as the carrier gas. The injection temperature was set to 250°C, and the GC oven programmed from 50 to 240°C in 8°C minute^{-1} increments. The MS was operated at an electron energy of 70 eV, with scanning conditions from 20 to 500 amu at 0.2 scan s^{-1}. The main products shown in Figure 2 were identified using reference standards, the others with their ion mass fragmentation pattern and the NIST database. Data processing was done using the Thermo Xcalibur software. Peak areas of compounds were obtained from an automatic peak detection method with subtraction of the baseline and noise reduction. Relative abundances of the main compounds were calculated from their area divided by the sum of all detected compounds' areas, allowing us to compare our samples and the relative abundance of each compound. Standard compounds were analyzed under the same conditions as the samples to validate the identification.

ICP-MS. Element content in water-liquid fractions were analyzed by Inductively Coupled Plasma-Mass Spectrometry (ICP-MS, ICAPQ, Thermo Electron, equipped with a collision cell) at the Institut IMBE, Marseille. Before analysis, samples (200 μl) were treated with nitric acid (10 μl) (Purissime, Sigma–Aldrich) and diluted by a factor of 2 with ultrapure water. Mg, Fe, Si, and K concentrations were measured at their masses of interest (m/z) of 24, 56, 29, and 39, respectively. Measurements were done in triplicate. Calibrations were done using external certified standards (Multielements, SCP Science).

Infrared Spectroscopy (FTIR). Reflectance analyses were done using a Brucker Vertex 70 FTIR spectrometer equipped with an attenuated total reflectance (ATR) device, ATR-Quest (Specac), operated at the PIIM laboratory. Spectra were acquired from 400 to 4000 cm^{-1} with a spectral resolution of 4 cm^{-1} and 32 scans at 1.6 mHz velocity. Background spectra were acquired with 62 scans at 1.6 mHz velocity every five measurements to ensure a good signal-to-noise ratio.

X-Ray Diffraction (XRD). The XRD measurements were carried out at the CINAM laboratory (Marseille, France), with a RigaKu RU6200BH device equipped with a high-gloss rotating Cu Kα radiation ($\lambda = 1.5418$ Å) anode and a 2D, flat image type, model Mar345 detector. For these measurements, the working power was 50 kV and the intensity was 50 mA with a 0.5 × 0.5 mm^2 beam size. XRD patterns were collected in quartz capillary containing crushed samples.

Electron Microscopy. Transmission electron microscopy coupled to energy dispersive X-ray spectroscopy (TEM-EDX) microanalyses were conducted at the CINAM laboratory on individual particles using a JEOL JEM 2011 TEM fitted with a Brucker X-Flash Silicon Drift Detector 5030. Data collection parameters for EDX analyses were set as follows: only

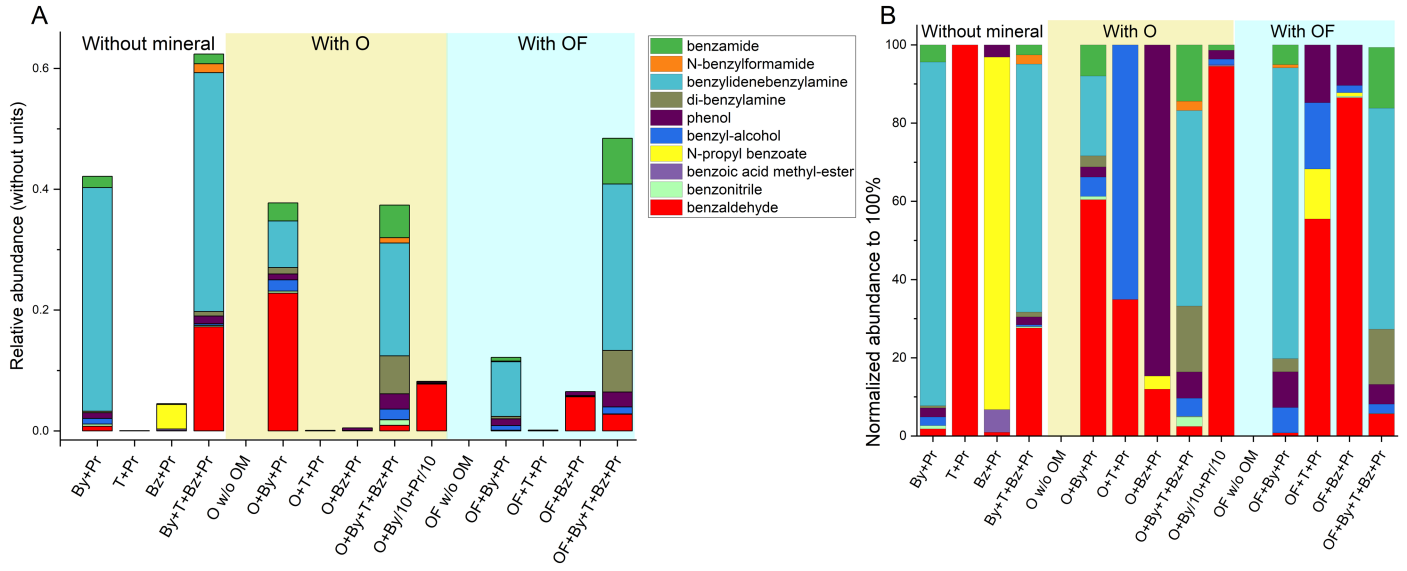

Figure 2. Major compounds detected by GC-MS in the samples after 45 days of hydrothermal alteration (Table A1). (A): relative abundances of these compounds (see methods), and (B) normalized relative abundances of compounds to 100%. By for Benzylamine, Bz for Benzoic acid, T for Toluene, Pr for Propanol, OM for organic matter, O for Mg-rich olivine, and F for Na-rich feldspar. *Relative abundance for sample O+By/10+Pr/10 has been multiplied by 10 for visibility in plot A. The effect of minerals is highlighted by compound relative abundances, which result in a decrease in the relative quantity (A) and an increase in the relative diversity (B).

hydroxylated phases were targeted with magnification of 50,000, 4L spot size, angular tilt of 20° toward the detector, time constant of 60 kcp s^{-1}, energy range of 40 keV, and corrected counting time of 30 s. The beam diameter was set to ~20 nm (200 Å) in order to reach the smallest particles. The constant beam density was ~63.5 pA cm^{-2}. Atoms O, Na, Mg, Al, Si, K, Ca, and Fe were quantified by applying the Bruker AXS MET line mark data quantification procedure (G. Cliff & G. W. Lorimer 1975). In this procedure, the acquired EDX spectra were corrected by background subtraction (Bremsstrahlung calculation), Gaussian deconvolution, and k factor corrections using values previously calculated on layered silicate standards with known homogeneous compositions (J. Berthonneau et al. 2014). Microphotographs of the sample were also acquired with a scanning electron microscope (SEM) JEOL JSM-7900F at 5 kV intensity.

Nitrogen Sorption at 77 K (BET). Textural characterization in terms of available specific surface area, porous volume, and external area was done by performing N_2 sorption at 77 K at the MADIREL Laboratory. The isotherms were obtained using either a GEMINI apparatus from Micromeritics or a BELSORP Max 1 from Microtrac for microporous samples. Before adsorption measurements, the samples were treated under vacuum at 100°C for 15 hr. BET (Brunauer–Emmett–Teller) formalism implemented with Rouquerol's criterium was used to obtain the specific surface areas. The total porous volume was calculated at $p/p^\circ = 0.99$ and the microporous volume was deduced using the *t*-plot method (J. Rouquerol et al. 2013).

3. Results

The pH of the liquid solution of each individual sample was qualitatively asserted after the reaction using pH paper (and therefore should only be used for relative comparison between the samples). The initial pH of all our solutions was measured close to the milli-Q water pH (6.5). Samples without minerals show that the organic molecules affected the pH by buffering the solution. For example, in experiments initially containing only benzoic acid (Bz), the final solution was acidic, while it remained circumneutral with toluene (T). The mineral-only samples exhibited an alkaline pH post-experiment, indicative of the release of metallic ions (e.g., Mg^{2+}, Fe^{2+}, Na^{+}, or Al^{3+}) and the probable consumption of H^{+}. Most of the organic solutions with minerals exhibited higher pH than the ones without (Table 1), attesting of the mineral effect. Small variations remained, as for the O+Bz+Pr of OF+Bz+Pr samples, having the lower pH (~6).

3.1. Liquid Phases

3.1.1. Organic Liquid (DCM Fraction)

The relative abundances of major compounds detected by GC-MS, confirmed with standard compounds, are shown in Figure 2. The types of organic molecules formed remain unchanged with or without minerals (Table A1), as no unique compounds were detected in the presence of minerals.

Propanol showed limited reactivity across all samples (Figures A1–A3), unlike benzyl molecules. The highest number of compounds (30) was identified in mineral-free samples with By+T+Bz+Pr (Figure 2, Table A1), serving as a reference for identifying molecules in other samples. In the mineral-containing mixtures, some minor peaks were absent or below detection limits compared to mineral-free samples (18 compounds for O and OF with OM, Figures A1–A3, Table A1). This suggests that the organic diversity of mineral-rich mixtures is reduced.

Notably, the distribution of compounds differed: mineral-free samples had one or two dominant compounds, whereas mineral-rich samples showed a more even distribution (Figure 2(B)). Benzylamine (By) was most reactive, forming the highest number of new compounds (Figure 2(A)). In mineral-free samples, By+Pr predominantly formed benzylidenebenzylamine, Bz+Pr yielded n-propyl benzoate, and T+Pr produced benzaldehyde, an oxidation product of toluene.

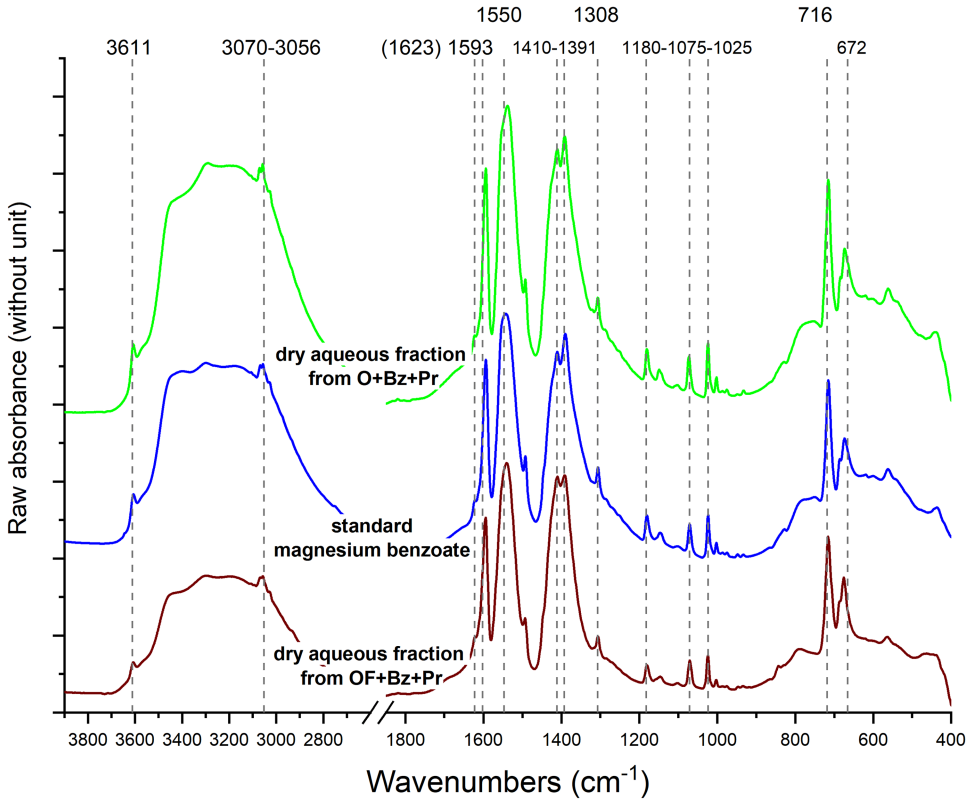

Figure 3. Infrared spectra of the dry aqueous fraction from the O+Bz+Pr sample compared to magnesium benzoate reference (bought from Aldrich) measured in the same conditions. Bz for Benzoic acid, Pr for Propanol, O for Mg-rich olivine, and F for Na-rich feldspar. The dashed lines provide the reference for the main absorption bands of standard magnesium benzoate, which are observed in the samples.

In the case of mineral samples, the relative abundance of these compounds is lower (Figure 2(B)), and more compounds such as phenol, benzyl alcohol, or benzamide are produced. To note, even if the toluene (T) and propanol (Pr) are the less reactive compounds here (likely due to the lack of functionalized group), a new distribution of molecules is observed in the mineral samples compared to mineral-free samples (however, with a relative quantification close to the detection limit). Overall, in mineral-containing mixtures (O and OF), compounds with more oxygen functionalities (e.g., benzaldehyde, phenol, and benzyl alcohol) were prominent, suggesting that minerals favored their formation.

3.1.2. Aqueous Fraction (Water Fraction)

Precipitation has been observed in the dry aliquots of the aqueous fraction from mineral-containing samples and has been analyzed by infrared spectroscopy (Figures 3, A4). No precipitates were observed in mixtures without minerals. The primary compound identified in sample O+Bz+Pr was a salt, namely magnesium benzoate ($C_{14}H_{10}MgO_4$), found in major proportions in O and OF samples containing benzoic acid (Figure 3). In Figure 3 is shown the comparison between the precipitates and the salt bought from Aldrich and measured in the same conditions as the sample. Many absorption features of the magnesium benzoate were found in common in the precipitates. Other unidentified species are formed in samples with benzylamine (By; Figure A4) and could correspond to another type of salts. ICP-MS analysis has been performed in the olivine series' experiments (Figure 4). The liquid fractions in mineral-free samples showed no detectable ions, confirming the origin of ions in our sample. In the sample without an organic molecule (O w/o OM), the concentrations of remaining ions in the solutions are low (e.g., Mg: 23.5–1.7 mg l^{-1}; Fe: 300–577 $\mu g\, l^{-1}$). The presence of an organic molecule modified Mg-rich olivine dissolution. Samples with benzoic acid (Bz) had the highest Mg concentrations (1700–1300 mg l^{-1}), while samples with benzylamine (By) had the lowest (0.8–8 mg l^{-1}). Lower benzylamine concentrations increased iron leaching (e.g., Fe: 8500 $\mu g\, l^{-1}$ for O+By/10+Pr/10 versus 415 $\mu g\, l^{-1}$ for O+By+Pr). Congruent dissolution was not observed here, as new minerals formed under all conditions. Mg/Fe ratios, typically 4–9, were significantly reduced under alkaline conditions (1–3 for O+By+Pr, O+By/10+Pr/10, O+KOH). The highest ratio (Mg/Fe = 887) occurred in mixtures with all organic compounds.

3.1.3. Mineralogy

All solid phases after alteration at 100°C show the formation of secondary phases, typically proto-phyllosilicates as evidenced by TEM/SEM (Figures 5, 7 and Figures A6, A7, and A11), FTIR (Figure 8), and XRD (Figures 6 and A8–A10). It should be noted that the analyses were carried out on the unwashed solid phases, which do not affect the mineralogical identification results.

3.1.3.1. Mineral Samples Produced without Organic Compounds

Mg-Rich-Olivine Series' Samples (O)

All the observed grains exhibited sheets, akin to those depicted in Figures 5 and Appendix Figure A6, with a notable lack of ordered structure, like poorly crystallized phyllosilicates.

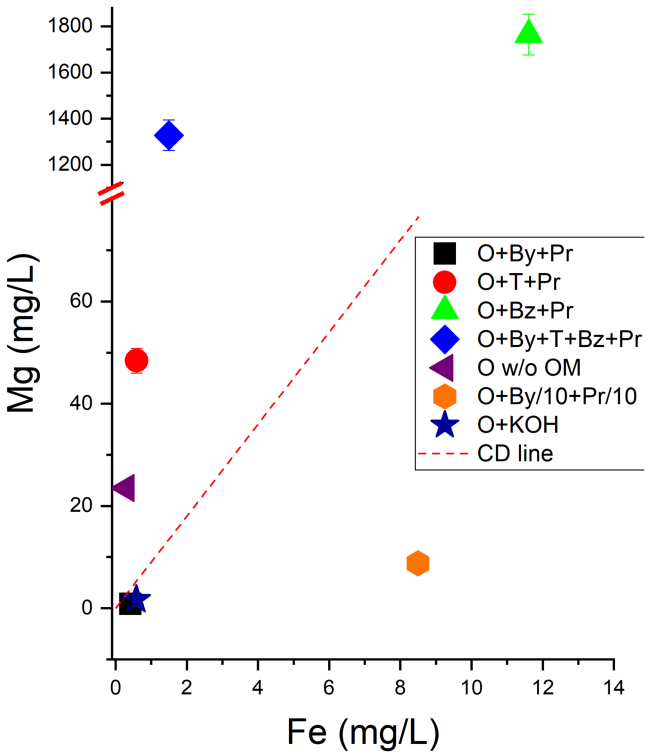

Figure 4. Analyses of Mg-rich olivine samples by ICP-MS, magnesium (Mg), and iron (Fe) concentrations in mg l^{-1} in the liquid phases after 45 days of hydrothermal alteration with Mg-rich olivine. Measurements were done in triplicate giving an average error bar of 5%. The symbols are larger than the error bars for small values. O for Mg-rich olivine, By for Benzylamine, Bz for Benzoic acid, T for Toluene, Pr for propanol, KOH for potassium hydroxide, and OM for organic matter. The red dashed line represent the theoretical congruent dissolution line of an olivine that would contain Mg:Fe = 90:10 mol-%. Evidence of the effect of organic compounds is indicated by the different concentration of residual ions in the solution after a 45 day period. This could be indicative of varying dissolution rates over the course of the experiment, or the precipitation of new phases with different compositions.

Chemical composition (obtained using TEM-EDX analyses) revealed that hydrothermal alteration of Mg-rich-olivine alone in our conditions (milli-Q water, 100°C, 45 days, anoxic environment) mainly formed secondary minerals close to serpentine composition, $(Fe,Mg)_3Si_2O_5(OH)_4$—a TO mineral (Figures 5 and A11). More precisely, in view of the wafer morphology by SEM (Figures 5(e) and (g)), and the position of the hydroxyl band in IR spectra (~3680 cm^{-1}—Figure 8), it was likely a lizardite-like mineral (J. Madejová et al. 2017; E. Fritsch et al. 2021). However, the band was broad and with at least shoulders at 3690 cm^{-1} and around 3600 cm^{-1}, indicating possible other phases, such as talc.

A broad diffraction line was observed at low angle on the XRD pattern, showing several maxima between 9.5 and 7.3 Å (Figure 6), typically corresponding to l 001 reflection of phyllosilicates. Among crystalline pattern from the initial mineral, new diffraction lines were observed (Figure A8), at 4.55, 3.65, ~2.66–2.58, and ~1.54–1.52 Å (Figure A8). Such broad diffraction peaks can be assigned to hk reflections of trioctahedral 1:1 serpentines, especially with the shoulder at 3.65 Å (S. W. Bailey 1988; E. Fritsch et al. 2021) but also to trioctahedral 2:1 smectites (O. Grauby et al. 1994). Additionally, the samples show signs of amorphous silicate phases in their TEM/SEM images (see Figures 5 and A6). These phases are also confirmed indirectly through the bump seen in the diffractogram baseline (Figure A8).

In alkaline condition with KOH, the final proto-phyllosilicates have a composition poorer in magnesium (richer in Si; Figures 5 and A11). The profile of the IR peaks shown a clear maximum at 3680 cm^{-1} and the additional band at 663 cm^{-1} (Figure 8), which match with bending vibrations of OH groups attached to octahedral Mg (Mg_3OH), like talc or saponite mineral (O. Grauby et al. 1994; J. Madejová et al. 2017; J. T. Kloprogge & C. P. Ponce 2021). XRD patterns showed diffraction lines at 4.55 and 1.52 Å, which is in agreement with the formation of more saponite-type phyllosilicate in alkaline conditions (O. Grauby et al. 1994; I. Criouet et al. 2023b; Figure A8).

Mg-rich olivine + Na-rich feldspar series' samples (OF)

TEM and SEM analysis revealed the presence of thin layers of disordered material covering Na-rich feldspar grains (Figures A6, A7), alongside completely altered grains with sheet structures.

The mineralogical composition of the secondary mineral was completely shifted to a very low concentration of magnesium but high concentration of aluminum as expected with the 3:1 Na-rich feldspar : Mg-rich olivine ratio (Figures 7 and A11). The final ratio of silica (Si) over aluminum (Al) ranged between 5:1 and 5:2. With XRD analysis, only a very shallow and broad peak at 4.55 Å can be observed among patterns from primary phases of Mg-rich olivine and Na-rich feldspar (Figure A9).

3.1.3.2. Mineral Samples Produced with Organic Compounds

In samples containing organic compounds, EDX analyses reveal that, on average, the elemental composition of the proto-phyllosilicates varies with the presence and nature of organic molecules, especially with benzoic acid and benzylamine (Figures 5–7). The closest samples to O and OF w/o OM, were the secondary phases formed with toluene and propanol molecules (O+T+Pr and OF+T+Pr; Figures 5–7).

Alteration of the minerals with Bz (O+Bz+Pr and OF+Bz +Pr) showed implementation of more iron in the structure than others (Figure 7). According to IR and XRD analyses, it was likely a saponite-type phyllosilicate formed from O+Bz+Pr, while an aluminum-smectite in sample OF+Bz+Pr (Figures IR 8, XRD A8–A9). In these samples (not washed) organic grains had also been observed by TEM (not shown here) and IR (Figure 8), and corresponded to magnesium benzoate compound (Figure A10). Nonetheless, for sample OF+Bz+Pr we had observed a mismatched, while magnesium benzoate was observed in the liquid phase (band at 3611 cm^{-1} corresponding to the stretching vibration of Mg–O, Figure 3). Since other ions are present in samples OF, such as sodium and calcium, we suspected the formation of new salts, such as sodium benzoate and/or calcium benzoate. These salts can have different hydration states and have a very similar IR spectra (SDBS database) but a diffraction line around 14.4 Å for monohydrated or dehydrated salts (A. Terakita & S. R. Byrn 2006; C. Butterhof et al. 2012). In addition, in sample OF+Bz+Pr we also observed some pure crystal of benzoic acid (diffraction line at ~10.6 Å; Figure A9; C. Butterhof et al. 2012).

Experiments with benzylamine (By) showed secondary phases with less iron and magnesium, closer to saponite-like composition for O+By+Pr with some talc, and montmorillonite-like for

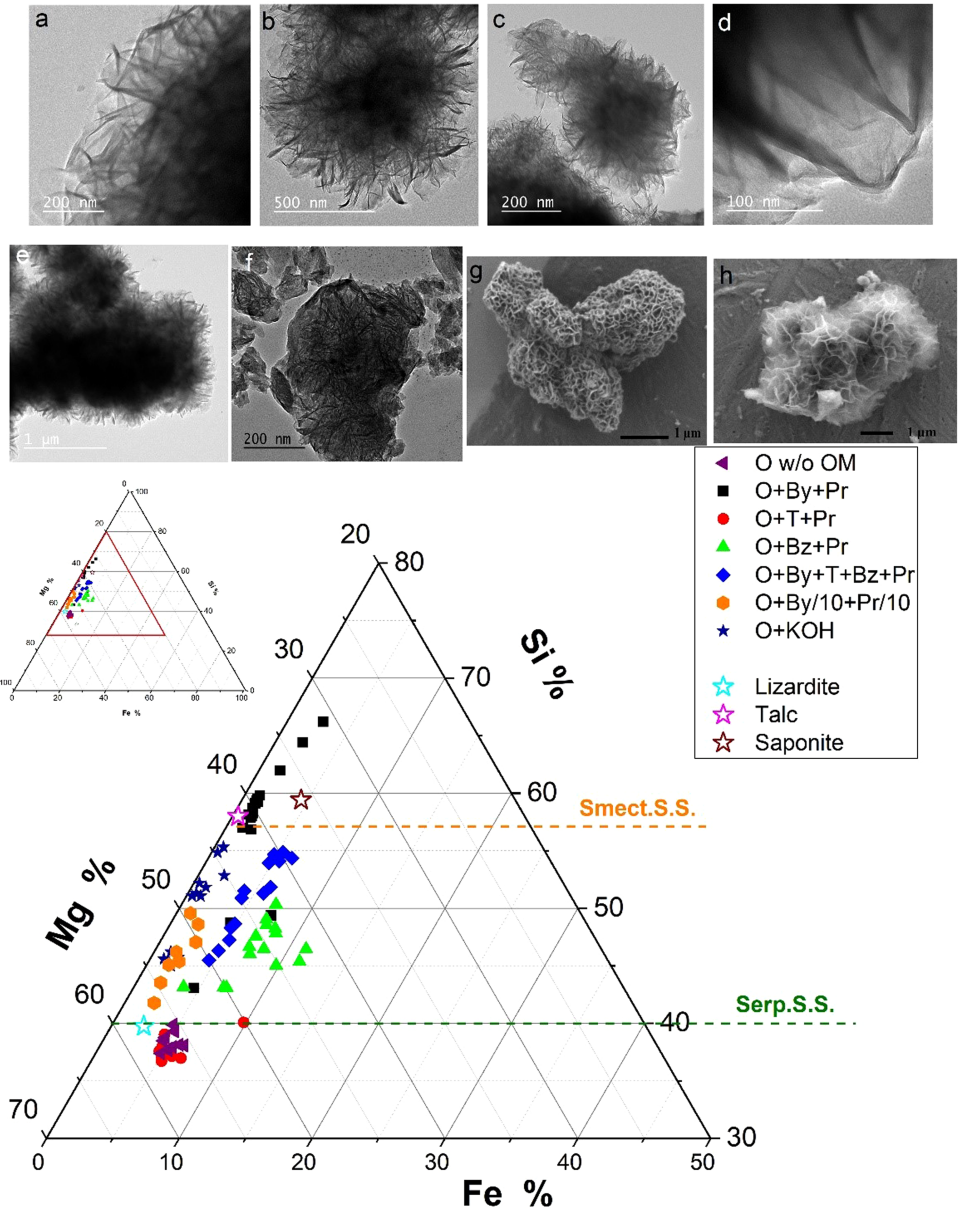

Figure 5. Chemical compositions of unwashed solid samples after 45 days of hydrothermal alteration at 100°C for the O series. O for magnesium-rich olivine, By for Benzylamine, Bz for Benzoic acid, T for Toluene, Pr for propanol, KOH for potassium hydroxide, and OM for organic matter. Images (a)–(f): representative TEM images of the samples showing the surface textures of grains recovered by proto-phyllosilicates, (a) from sample O+By+Pr; (b) from sample O+T+Pr; (c) from sample O+Bz+Pr; (d) from sample O+By+T+Bz+Pr; (e) from sample O w/o OM; and (f) from O+By/10+Pr/10. Images (g)–(h) are SEM analysis, (g) from sample O w/o OM and (h) from sample O+By+Pr. Below is the ternary diagram in Si, Mg, and Fe (at. %) showing the composition of secondary phases obtained by EDX analysis. For each sample, at least 10 different locations onto these phyllosilicate morphologies were analyzed and are reported in the same color for each sample. Orange and green lines are the solid solution lines of ideal smectite-type (Smect. S.S.) and serpentine-type (Serp. S.S.) phyllosilicate compositions. All the samples fall between and around these lines, with a variable magnesium content. Example of the composition of known minerals (end-members) are given for comparison (lizardite and talc from Ruff database, and saponite from O. Grauby et al. 1994). Errors on the measurements are <10%. Organic compounds, especially benzylamine and benzoic acid, clearly affected the composition of the phyllosilicate that is formed from olivine alteration in our conditions.

OF+By+Pr; Figures 5–7). Interestingly, a lower concentration of benzylamine in the initial solution (sample O+By/10+Pr/10) was associated with the formation of secondary phases with a higher concentration of magnesium, resembling a phyllosilicate in between saponite and serpentine-type and closer to phyllosilicate formed in sample O+KOH (Figure 5). To note, a broad diffraction peak at 15.6 Å is observed for sample O+By+Pr (Figure 6), which could correspond to the adsorption of organic matter in the interlayer structures. Organic bands are indeed observed by IR between 1700 and 1300 cm^{-1} (CH, NH, OH, C=C, C–N groups) for these unwashed samples O+By+Pr, O+Bz+Pr, and O+Bz +T+By+Pr (Figure 8).

3.1.4. Organic Content in Solid Phases

The elemental analysis of the solid materials were conducted before and after washing with solvents (see method) to assess the percentage of slightly sorbed organic phases from adsorbed organic phases with the minerals (Table 2).

In all cases, half of the carbon and nitrogen found before washing had only been slightly absorbed by the minerals

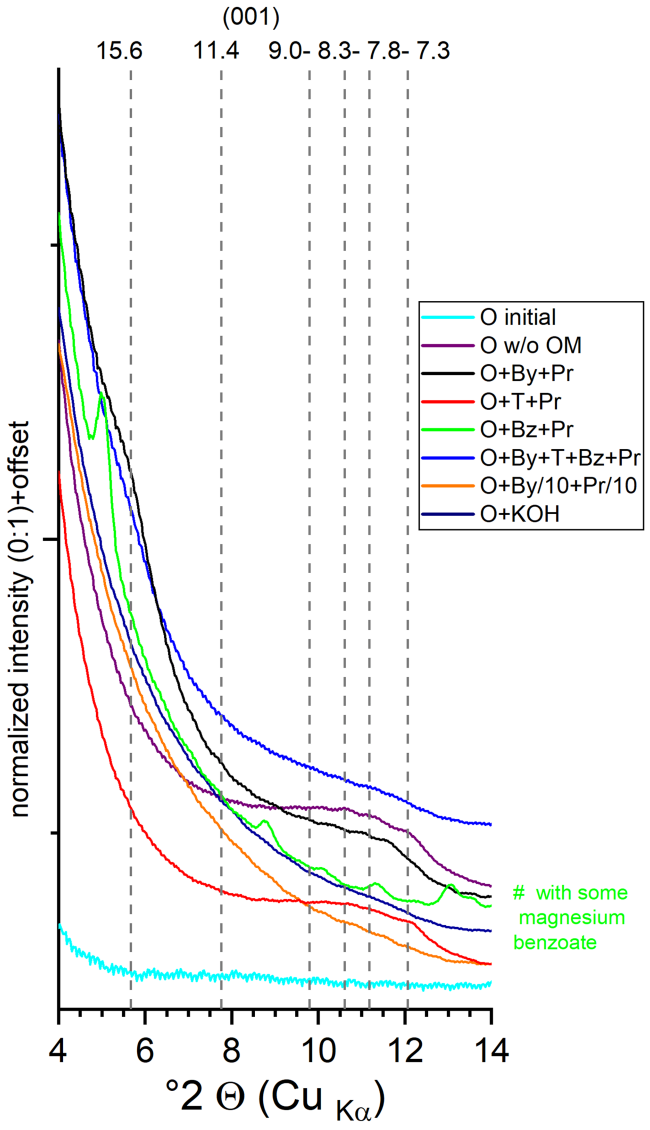

Figure 6. XRD pattern between 4 and 14° 2 Θ of unwashed solid samples after 45 days of hydrothermal alteration at 100°C for the O series. O stands for magnesium-rich olivine, By for Benzylamine, Bz for Benzoic acid, T for Toluene, Pr for propanol, KOH for potassium hydroxide, and OM for organic matter. New diffraction lines, not seen in all patterns, are highlighted with their corresponding interatomic distance in Å, which likely corresponds to l(001) reflections of clay minerals. All the samples showed an increase in the baseline and small but visible diffraction lines in this part of the XRD pattern. This suggests that there are poorly crystallized phyllosilicates present.

(Table 2). Nonetheless, after washing, there was still up to 7 wt% of carbon measured for sample O+By+T+Bz+Pr and 4.5 wt% of carbon for sample OF+By+T+Bz+Pr. The values represented 8.9 wt% and 5.7 wt% of the initial carbon introduced into the system, respectively. Interestingly, carbon and nitrogen abundances in OF samples were overall inferior to O samples (with or without washing). Nonetheless, a higher quantity of nitrogen was adsorbed with both mineral phases (up to 14%wt for OF+By+T+Bz+Pr).

3.1.5. Surface Area (BET) and Porosity

Adsorption–desorption isotherms for samples are given in Figure 9 (and individually in Figures A12 and A13). For samples containing organic matter, the adsorption measurements were made before and after the washing procedure (see Methods), but only two samples showed some variations (Figure A14).

Initial Mg-rich olivine and feldspar showed a Type II isotherm in the IUPAC classification (M. Thommes et al. 2015), in agreement with the nonporous characteristic of the starting minerals (Figure A12). Their BET surface areas were found equal to $\sim 7\ m^2\ g^{-1}$.

With the formation of secondary phases in the samples, the isotherms showed modified hysteresis between the absorption and desorption branches, in agreement with porous structures like phyllosilicates (L. J. Michot & F. Villiéras 2013; Figure 9(A)). As first sight, isotherms might be assigned to Type IV isotherms (mesopores) but the absence of saturation plateau was not consistent with this type of isotherm. Moreover, a more pronounced uptake was observed at low p/p° and the inflexion point observed in the log scale (Figure 9(B)) was indicative for the presence of micropores. These adsorption isotherms could thus be described as a combination of Type I(b) (microporous) and Type II(b) (nonporous or macroporous) isotherms, with an H4-type hysteresis loop (M. Thommes et al. 2015).

Both the BET surface area and the total adsorbed volume at p/p° were much higher for the samples after hydrothermal alteration (Figure 10—up to 330 $m^2\ g^{-1}$). The majority of the porosity is constituted by micropores (<5 nm) and accounted for up to 70% of the pore area (Figure 10). Of note, the OF series' samples all exhibited lower BET areas and porosities.

Five samples showed a smaller hysteresis than others and almost no micropores (O+By+Pr; O+By+T+Bz+Pr; OF +By+Pr; OF+Bz+Pr; OF+By+T+Bz+Pr). The adsorption branches have the same Type II(b) character than initial olivine, but a small H3 type hysteresis is observed at the desorption. The BET area for these samples are only lightly higher than the initial O or F samples (Figure 10). The presence of the hysteresis nonetheless confirmed layer structures of phyllosilicates (L. J. Michot & F. Villiéras 2013), but the microporosity is nearly not existent compared to other samples (Figure 10). It is notable that these samples contain the highest concentration of carbon (see Table 2), which may be the source of this nonobservation of porosity. Indeed, two samples showed different N_2 adsorption–desorption before and after washing, clearly showing an increase in BET area and porosity with washing due to the release of OM (Figure A14, Table 2).

4. Discussion

4.1. Mineral Impact on Organic Distribution

The results of our experiments demonstrate that the diversity of organic matter is increased in hydrothermal systems at 100°C. We have observed products, which could be the result of hydrolysis (reaction of molecule with water) like benzaldehyde formation from benzoic acid, but also products of oxidation, such as benzamide from benzylamine or dehydratation reactions like benzyl alcohol formation from benzoic acid or even polymerization like the dibenzylamine and the N-benzylidenebenzylamine formation from benzylamine (Figure 1). Hence, the formation of the new molecules cannot be attributed solely to hydrolysis (reaction with water); rather, they are the consequence of complex chemical reactions occurring during the experimental time with and without minerals. Such increased diversity due to hydrothermal

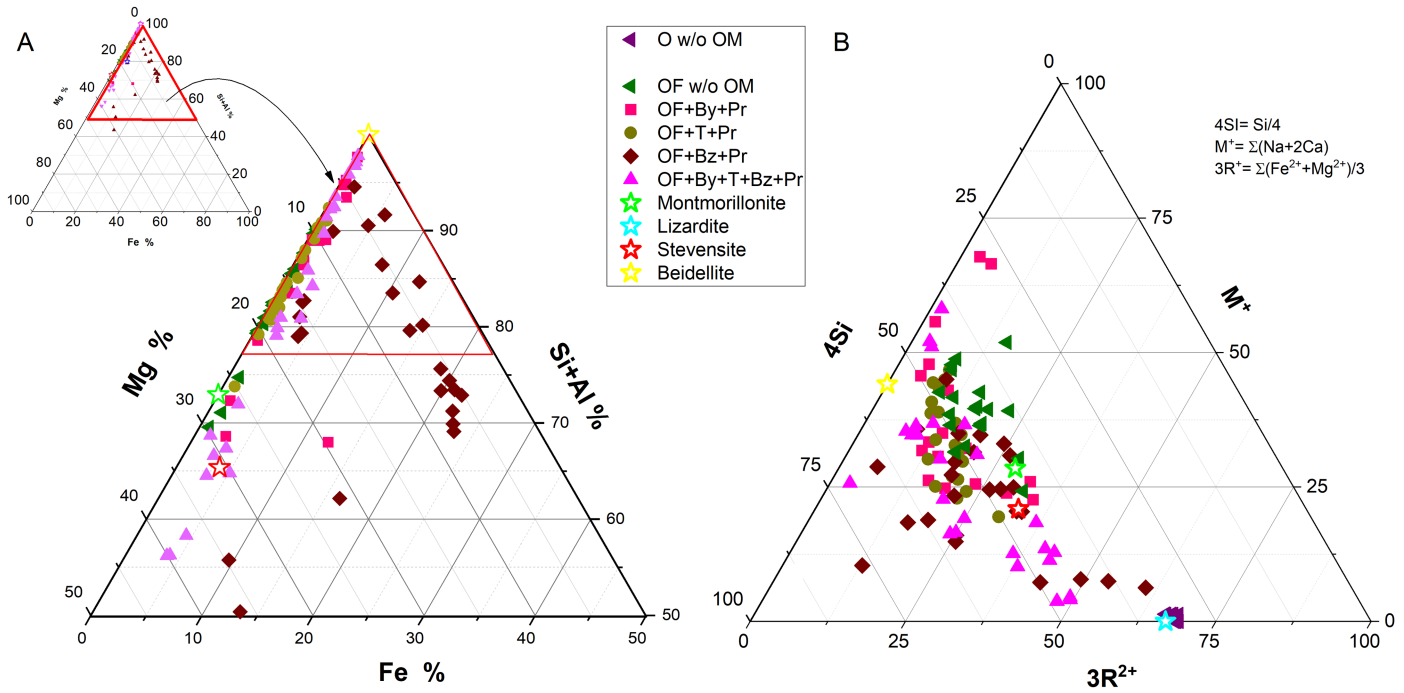

Figure 7. Chemical compositions of phyllosilicates, analyzed by TEM-EDX, observed in OF series samples after 45 days of hydrothermal alteration at 100°C. (A) Ternary diagram in the Fe/Mg/Si+Al representation and (B) ternary diagram in the 4SI, M^{+}(Ca+Na+K), and $3R^{2+}$(Fe+Mg) representation (A. Meunier & B. Velde 1989; A. Meunier 2005). O for magnesium-rich olivine with F sodium-rich feldspar and organic molecules, By for Benzylamine, Bz for Benzoic acid, T for Toluene, Pr for propanol, and OM for organic matter. For each sample, at least 10 different locations were analyzed and are reported in the same color for the sample. Example of the composition of known minerals (end-member), appropriate to our study are given for comparison (high charge montmorillonite and beidellite from A. Meunier & B. Velde 1989, lizardite data from the Ruff database, and stevensite from the webmineral database). Errors on the measurements are <10%. Organic compounds, especially benzoic acid, clearly affected the composition of the phyllosilicate that is formed from olivine and feldspar alteration in our conditions.

alteration has been observed in previous abiotic systems (V. Vinogradoff et al. 2018; Y. Isono et al. 2019). Nevertheless, our experiments demonstrate a change in diversity and lower relative abundance of organic compounds in the presence of minerals, attesting of interactions with the mineral (Figure 2(A)). Interestingly, such a decrease in abundance after hydrothermal alteration has already been reported in other studies based on phyllosilicate or amorphous gel phases reacting with different organic compounds (hexemathylenetatramine, RNA, formaldehyde; P. Jacquemot et al. 2019; V. Vinogradoff et al. 2020; J.-C. Viennet et al. 2022).

Hints of several different chemical interactions between the aromatic compounds and the minerals are postulated in our samples based on previous studies (M. Schoonen et al. 2004; G. Lagaly et al. 2013; M. Kleber et al. 2015, 2021; V. Vinogradoff et al. 2020). The observation of magnesium benzoate and potentially other salts (Figures 3 and A4) can be related to the chelation process, which likely occurred at the surface of our silicates (S. V. Golubev et al. 2006; M. Kleber et al. 2015; C. Serra et al. 2024). For example, in the case of benzoic acid (Bz), the formation of chelate may inhibit reaction of Bz, in agreement with the lower relative abundance of compounds formed in this sample with minerals (Figure 2). It is notable that benzoic acid has not been extracted in the DCM fraction (almost undetectable in the GC chromatogram), likely due to the formation of the chelate, while it is clearly discernible in GC-MS chromatograms of samples without minerals (Figures A1–A3). The physisorption process at the surface, acting as catalyst or oxidant can explain the observation of more saturated and oxidized compounds in the organic fraction (Figure 2, Table A1; M. Schoonen et al. 2004). The 10% iron content of the olivine may have indeed facilitated some redox reactions (S. Peters et al. 2023), but further analysis is necessary to ascertain the Fe^{2+}/Fe^{3+} ratio in our experiments.

Our results suggest also evidences of chemi-sorption at the surface and within the interlayer space of the phyllosilicates, especially those coming from olivine alteration. The total organic carbon remaining with some solid residues (after washing) can be directly related to the nonexistent porosity in the same material (Figures 9–10), confirmed by washing procedures releasing porosity in only two samples (Figure A14). The disordered structuration of sheets, made during the experiments, may have created an environment conducive to the incorporation of some organic molecules. Indeed several clues point to the formation of protophyllosilicates, poorly crystallize and with composition intergrown in disordered sequences. BET signatures is in agreement with the formation of highly porous mineral and such characteristics have been observed particularly for pillared interlayered clays (PILCs; H. J. Chae et al. 2001; J. A. Cecilia et al. 2018) having large interlayer space and microporosity. This chemical sorption can be attributed to Lewis or Brønsted acid sites, which are more pronounced in the interlayer space of pillared clays (J. A. Cecilia et al. 2018) and to which aromatic moieties may sorb (F. Kooli & W. Jones 1997). In addition, the disordered packing of phyllosilicate sheets, intergrown as observed in our experiments, has been put forth as a potential catalyst for OM synthesis in serpentinized rocks (B. Ménez et al. 2018).

Among the molecules we selected for our study, the most reactive one appears to be benzylamine (By), the nitrogen-bearing molecule, with evidence of reactions such as hydrolysis or nucleophilic addition. Given the alkaline pH of the solution with By, nitrogen-bearing molecules are

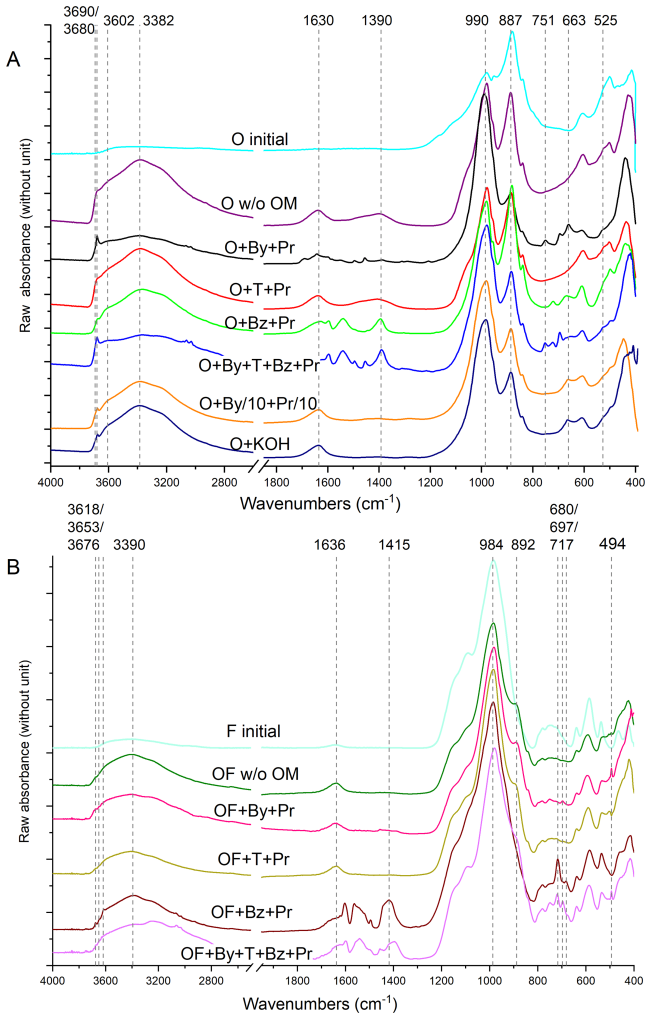

Figure 8. Infrared spectra of silicate residues (no washing) after aqueous alteration at 100°C with or without organic matter for the O series (A) and the OF series (B). O for magnesium-rich olivine, F for Na-rich feldspar, By for Benzylamine, Bz for Benzoic acid, and T for Toluene, Pr for propanol, KOH for potassium hydroxide, and OM for organic matter. New bands corresponding to phyllosilicates are clearly observed on the solid residues, in the O series (A) ν(OH) at 3680 cm^{-1} (hydroxyls-likely Mg–OH), δ(OH) 1630 cm^{-1} (interlayer water), as well as modification of the Si–O stretching band (ν(Si–O)) at 990 or 887 cm^{-1}) and new Mg–OH or Fe–OH bending modes 751, 663, and 525 cm^{-1}; in the OF series (B) νOH at 3618, 3653, and 3676 cm-1 (hydroxyls), δOH 1636 cm^{-1} (interlayer water), as well as modification of the Si-O stretching band (νSi–O at 984 or 892 cm^{-1}) and new bands at 680, 697, 717, and 494 cm^{-1}. Peaks of organic matter near 1700–1300 cm^{-1} are observed for some samples with By and Bz, indicating the presence of OM, in agreement with elemental analysis (Table 2). In both experimental series, the infrared spectra showed clear changes to the structural bands of the starting silicates, and the formation of minerals like phyllosilicates due mainly to the hydroxyl bands.

susceptible to bear positive charges (under the form of R-NH_x^+ since they have a pka within alkaline pH range) and so may be more favorably adsorbed on the possible negatively charged surfaces of the secondary phyllosilicates (B. B. Velde & A. Meunier 2008; M. Kleber et al. 2015). This could explain the yield of 5–14 wt% of N in the final solid (Table 2). The presence of feldspar has decreased the nitrogen adsorption, likely due to the production of different phyllosilicates' compositions and abundance, but also because less compounds are produced in OF mixtures (Figure 2—Table 2). Nonetheless, the yield of nitrogen adsorbed with mineral was equal or higher than carbon in the final solids, thus suggesting a preferential adsorption of nitrogen molecules. It should be noted that nitrogen can also be present in inorganic forms, such as NH_4^+ with phyllosilicates under our conditions, but no observations have been made here. This property of nitrogenous molecules, seen also in other experimental studies from different OM with phyllosilicates (J.-C. Viennet et al. 2019; I. Criouet et al. 2023a; C. Serra et al. 2025), is worthy of particular attention with regard to the chemistry of abiotic systems, as it may provide insights into the reactivity and availability of nitrogen with phyllosilicates.

Overall, our experiments show that the presence of minerals modifies the final distribution of organic compounds, may favor specific chemical pathways, but likely reduces the diversity formed. Also, if high concentration of reactive organic molecules are present during hydrothermal alteration of silicates, some are likely to be trapped within the newly formed phyllosilicates, especially nitrogen-bearing molecules.

4.2. Secondary Minerals Differ by Organic Molecules

4.2.1. Nature of the Secondary Minerals Without Organic

Samples without organic molecules served as controls to determine the composition of secondary phyllosilicates formed from olivine and feldspar under our hydrothermal alteration conditions.

Spectroscopic and microscopic analyses revealed that altered Mg-rich olivine exhibited signatures of hydroxylated mineral structures, likely proto-phyllosilicates, indicating efficient transformation under the applied conditions (100°C, anoxic atmosphere, 45 days). This transformation was likely enhanced by the small grain size of the starting material (<10 μm, Figure A5). However, the exact chemical formula of the newly formed mineral could not be determined due to the large compositional variability (Figures 5 and 7) and uncertainty in cation assignment, particularly for iron (Fe^{2+} or Fe^{3+}) (W. A. Deer et al. 2013).

In our conditions, under anoxic gas, with ultra-clean water at 100°C and W/R of 20, we have observed the formation of a mixture composition close to serpentine (lizardite type) from the olivine protolith without OM (Figures 5 and A11). The transformation of olivine into a serpentine phyllosilicates is a well-known process happening even at low temperatures (B. W. Evans 2004; A. Neubeck et al. 2011, 2014; E. H. Oelkers et al. 2018). The most abundant secondary phases–but also the most difficult to quantify–are the amorphous silica-rich phases as hinted from the XRD pattern (Figures A8, A9) and infrared signatures (Figure 8). Finally, the microporous structure observed in absorption analysis (Figures 9–10), combined with diffraction lines between 9.5 and 7.3 Å (Figure 6) and the variability in secondary phase compositions, suggests the presence of intergrown sequences. The high BET surface area and the porous volume are indeed matching with pillared interlayered clays (PILCs) in structure (H. J. Chae et al. 2001; J. A. Cecilia et al. 2018) and interstratified or intergrown clays in composition (F. Veniale & H. W. Van der Marel 1968; A. Alietti & J. Mejsner 1980; A. Steudel et al. 2017). In other words, a complex intercalation of various poorly crystalized serpentines (and likely some smectites) and amorphous silicates have been formed in our samples without OM, ending in irregularly mixed-layer minerals that increase the microporosity (illustration in Figure 11). Such structuration

Table 2
C, N, and H Composition (wt%) of the Solid Residues after 45 Days of Experiments, Before and After Washing Procedures (See Methods)

		C wt% ± 0.2		N wt% ±0.02		H wt% ±0.1			
	Sample Names	Before	After	Before	After	Before	After	C Yield wt%[a]	N Yield wt%[a]
Raw sample	O	0.21	/	0	/	0.76	/	…	…
	F	0.16	/	0	/	0.64	/	…	…
Samples after 45 days of alteration	O+By+Pr	8.49	4.55	0.67	0.36	1.75	1.74	13.9	9.4
	O+T+Pr	0.38	0.2	0	/	1.98	1.95	…	…
	O+Bz+Pr	3.33	0.77	0	/	1.69	1.8	2.4	0
	O+By+T+Bz+Pr	15.13	6.96	1.16	0.47	2.08	1.90	8.9	12.3
	O w/o OM	0.24	/	0	/	2.04	/	…	…
	O+By/10 +Pr/10	0.22	0.15	0.07	0.02	1.79	1.81	…	…
	O+KOH	0.07	/	0	/	1.92	/	…	…
	OF w/o OM	0.10	/	0	/	0.88	/	…	…
	OF+By+Pr	2.63	1.80	0.45	0.31	0.99	1.05	5.5	8.1
	OF+T+Pr	0.06	/	0	/	0.79	/	…	…
	OF+Bz+Pr	2.86	2.34	0	0	1.05	0.93	7.3	0
	OF+By+T+Bz+Pr	9.5	4.47	1.02	0.56	1.3	1.3	5.7	14.7

Note. C and N yield in wt% from the initial carbon and nitrogen abundance in the sample is also reported for samples after the washing steps. Initials refers to components, O for magnesium-rich olivine, F for Na-rich feldspar, By for Benzylamine, Bz for Benzoic acid, T for Toluene, Pr for propanol, KOH for potassium hydroxide, and OM for organic matter. The / sign means no new measurement.
[a] After the washing steps.

has been observed on natural setting (V. A. Drits 1997), for example, with talc-saponite composition on Earth (F. Veniale & H. W. Van der Marel 1968; A. Alietti & J. Mejsner 1980; A. Steudel et al. 2017) or serpentine–saponite composition in meteorites (K. Tomeoka & P. R. Buseck 1988; A. J. Brearley 1995).

By mixing olivine with feldspar in the starting material, new mineral compositions were formed, typically with higher aluminum content (Figure 7), although there is less variability in their composition between samples, the composition of the final phyllosilicate is spammed over a wider range of Al-dioctahedral and trioctahedral smectites (Figure 7—A. Meunier & B. Velde 1989; A. Meunier 2005). Na-rich feldspar dissolution is controlled by surface area, time, and pH conditions (M. Lagache 1976; S. Gudbrandsson et al. 2014), and produced kaolinite ($Al_2Si_2O_5(OH)_4$ and bohemite (AlO(OH); M. Lagache 1976), but when mixed with olivine, Al-rich clays are expected (R. Oyanagi et al. 2017). Here in our conditions, feldspar dissolution was likely limited, as seen by TEM and XRD analyses (unaltered grains and XRD pattern), consistent with the relatively higher dissolution rates of olivine versus feldspar (M. Heřmanská et al. 2022). Nonetheless, this was sufficient to incorporate at least 20% of Al in the smectite-type formed (Figure 7).

In both series, the resulting solutions after 45 days of hydrothermal alteration exhibit alkaline pH (around 8–9), due to the dissolution of the primary silicates that consumes H^+ ions while releasing cations (Al, Mg, Fe, Na, Ca) into the solution. Newly formed grains most likely exhibit an "onion"-type morphology, with a center of still nonaltered olivine/feldspar, then a layer of amorphous phases (similar to a gel) and proto-phyllosilicate layers on top or vice versa (D. Daval et al. 2011).

4.2.2. Nature of the Secondary Minerals with Organics

In general, the secondary phases that formed in our conditions, with organic matter span a large range of compositions (Figures 5–7–A11). These included serpentine-like materials such as lizardite, which formed from the Mg-rich olivine protolith with neutral organic molecules (T and Pr), similarly to secondary phases formed without OM. Other compositions included Mg-smectites with trioctahedral layers, such as saponite/talc, which formed when the phyllosilicates were mixed with acid (Bz) or basic (By) organic molecules. The presence of aluminum-bearing phyllosilicates, with likely mixed dioctahedral and trioctahedral layers such as aluminum smectites (composition closed to montmorillonite or beidellite), is evidenced when sodium-rich feldspar is present in the protolith with organic molecules (Figures 7, 8, and A11). All clays produced are likely mixed layers or interstratified smectites, as seen from their nitrogen adsorption–desorption profiles (Figures 9–10) and XRD pattern at low angle (Figure 6).

The impact of organic molecules seen from our study can be attributed to a combination of at least three parameters: (1) the pH of the solution, which varied due to the organic molecules (Table 1; Figure 4); (2) the chelation effect: depending likely on the concentration and nature of the organic molecules (Figure 3, A4 and A10); (3) chemi and physisorption of molecules at the surfaces, edges, and interlayers (Table 2, Figures 9–10).

The first two parameters can be combined. Indeed, organic acids are known to modify the dissolution rates of olivine or plagioclase, combining a pH effect and chelating ligands (R. A. Wogelius & J. V. Walther 1991; S. A. Welch & W. J. Ullman 1993; J. I. Drever & L. L. Stillings 1997; O. S. Pokrovsky & J. Schott 2000; E. H. Oelkers 2001; S. Gudbrandsson et al. 2014; E. H. Oelkers et al. 2018). Although the pH drop is not significantly high (Table 1), it is likely that the formation of chelates with organic molecules has also modified the dissolution of the starting material (Figure 4; R. A. Wogelius & J. V. Walther 1991). The samples with Bz are in agreement with the highest ion dissolution (as evidence by the remaining ions Figure 4), explaining the higher incorporation of iron in the final phyllosilicates (Figures 5, 7). In alkaline conditions, pH has less of an effect (S. Gudbrandsson et al. 2014; E. H. Oelkers et al. 2018).

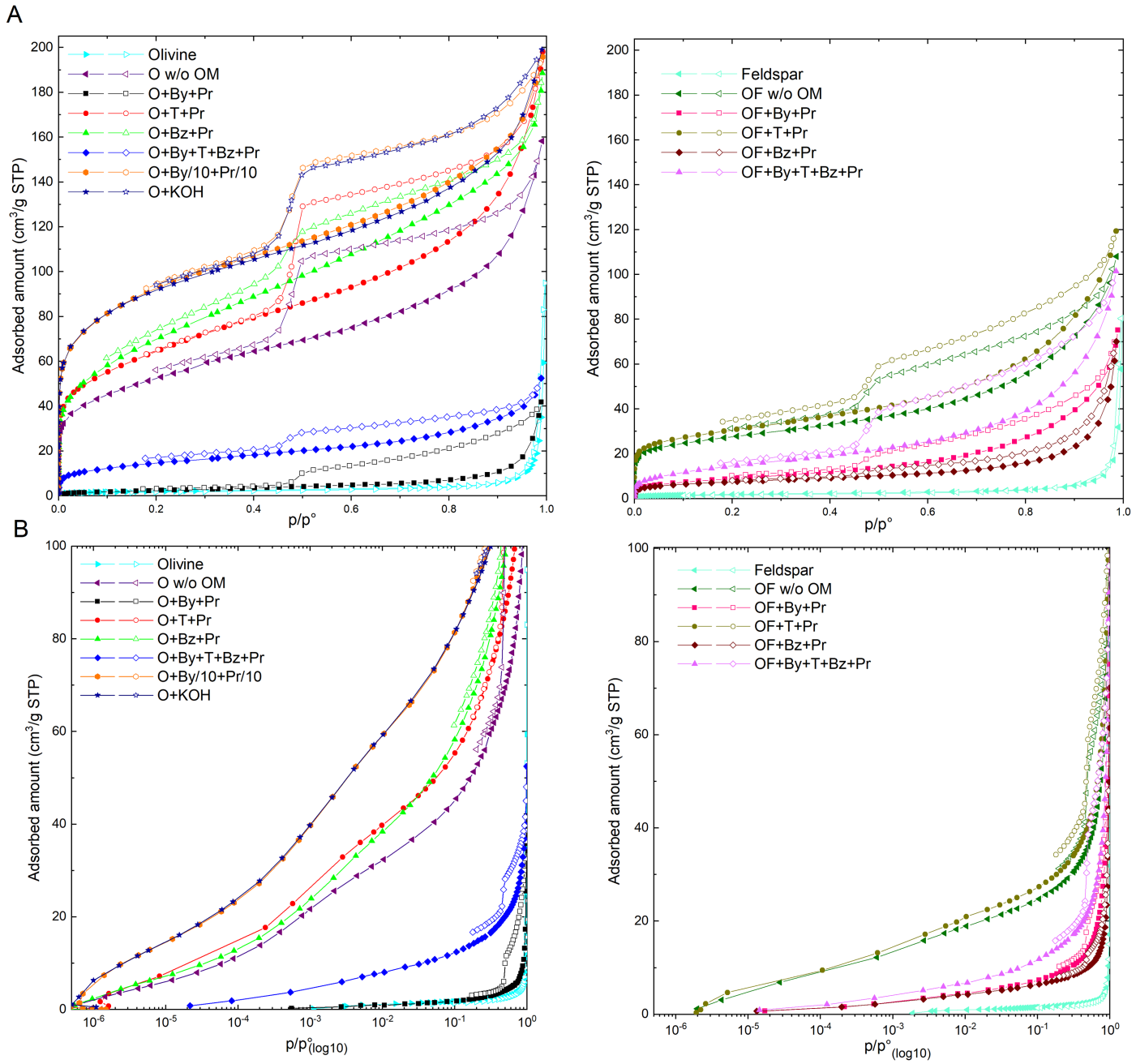

Figure 9. (A) N_2 adsorption–desorption isotherms measured at 77 K for the washed samples after 45 days of hydrothermal alteration at 100°C for Mg-rich olivine and Na-rich Feldspar with olivine series (O and OF). (B) Same isotherms plotted in logarithm scale in order to make more visible the N_2 uptake at low pressure and the inflexion points characteristic of microporosity of the samples. For both figures, O stands for magnesium-rich olivine, F stands for feldspar, By for Benzylamine, Bz for Benzoic acid, T for Toluene, Pr for Propanol, KOH for potassium hydroxide, and OM for organic matter.

Therefore, in our samples with By, it is likely that the formation of chelates disrupted the mineral's dissolution since different result are found between the basic sample (O+KOH) and the organic-basic sample (O+By+Pr). It seems reasonable to posit that the pH and the presence of chelates have also directly affected the porosity of the final material. This is evidenced by the increased microporosity observed in some samples (see Figures 9–10). Finally, the concentration of the organic molecules is also an important factor, as seen with sample O+By/10+Pr/10, having an intermediate composition and properties between the high concentrated sample (O+By) and the sample without OM. Such observations confirm the effect of OM even at low concentrations (25 mM). The other parameters, not tested here, that can influence mineral dissolution, are the temperature, the water to rock ratio, the grain size, and the partial pressure of CO_2 or O_2 as shown in previous studies (R. A. Wogelius & J. V. Walther 1991; D. Daval et al. 2011; N. C. Johnson et al. 2014; A. Gaudin et al. 2018; E. H. Oelkers et al. 2018). Since the temperature, grain size, water-to-rock ratio, atmosphere, and duration were identical for both series in this study, the only factor influencing mineral dissolution and the subsequent crystallization of new phases was the presence of high concentrations of organic molecules and their intrinsic properties.

The third parameter, the chemi/physi-sorptions of organic compounds is the most difficult to predict, since it is highly

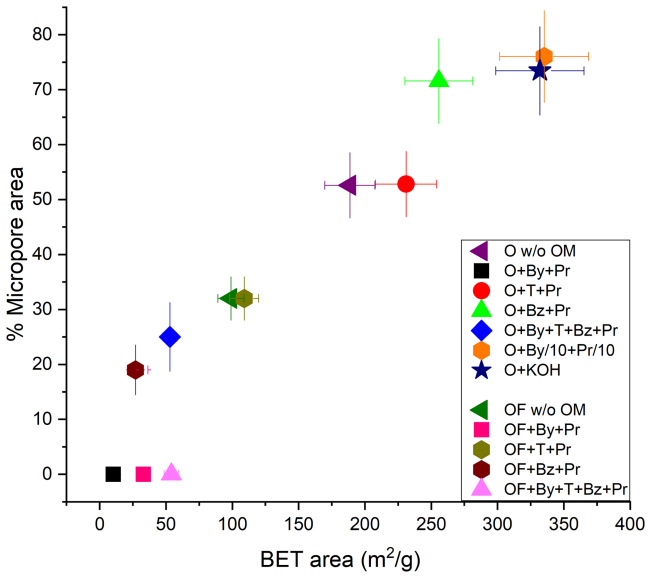

Figure 10. Specific surface area (BET) of the washed samples after 45 days of hydrothermal alteration at 100°C vs. micropore area contribution to the BET surface area in percent. Analyses were performed two times and error bars are 10% for both areas, except for the small micropore area where the error is higher, 20%. O stands for magnesium-rich olivine, F for Na-rich feldspar, By for Benzylamine, Bz for Benzoic acid, T for Toluene, Pr for Propanol, KOH for potassium hydroxide, and OM for organic matter.

dependent on the nature, properties, and quantity of organic compounds. Nonetheless, as shown here, a large adsorption of compounds for both series O and OF is detected (Table 2–after washing). We propose that the high quantity of organic matter (OM) detected in the five samples with small hysteresis and negligible microporosity (Figures 9–10) is chemisorbed within the pores and interlayer spaces. Based on the observed step in the hysteresis curve, assumed to correspond to the interlayer space, it can be inferred that the organic molecules have filled these spaces in the samples. This is consistent with the comparison of samples before and after the washing procedure, which revealed an increase in the step height and overall porosity (Figure A14). It is worth noting that the concentration of OM in the solution is a key factor, as the sample with the lowest OM concentration (O+By/10+Pr/10) did not exhibit such porosity saturation.

This quantity of material chemisorbed with phyllosilicates and likely the amorphous phases is among the highest in related laboratory experiments (J.-F. Lambert 2008; C. Feuillie et al. 2013; U. Pedreira-Segade et al. 2016; P. Jacquemot et al. 2019; V. Vinogradoff et al. 2020; J.-C. Viennet et al. 2022; C. Serra et al. 2025). This observation may be attributed to the in situ formation of the secondary phases (proto-phyllosilicates and amorphous phases), which differs from the conditions of other studies, but also to the nature of the organic compounds themselves and their initial concentration in the system.

The results of our study demonstrate that aromatic organic molecules have exerted a distinctive influence on the dissolution of the silicate, as well as the crystallization and porosity of the secondary mineral. Their nature and concentration have led to an enhanced probability of entrapment, which could prove advantageous for the preservation of these molecules (M. Kleber et al. 2015; J. D. Hemingway et al. 2019).

4.3. Implications for Early Mars–Earth Organic-mineral Systems

The past decades have highlighted the occurrence of organic compounds in many different past or present hydrothermal environments (Mars, Ceres, and icy moons). As seen from our study, organic-mineral interactions can be as diverse as the conditions are different (temperature, salts, pH, and composition). Such mixtures can hence either blur, help, or prevent OM detection.

Our generic alteration experiments may apply to several past Mars hydrothermal environments, where organic matter is currently searched (M. Millan et al. 2022; S. Sharma et al. 2023). Although the temperature of our experiments is representing hydrothermal environments, on a long timescale we do not expect the alteration products, especially the minerals to differ significantly from the lower-temperature aqueous reactions on early Mars (E. M. Hausrath et al. 2008; A. Gaudin et al. 2011), or in terrestrial aqueous systems (D. R. Janecky & W. E. Seyfried 1986; O. S. Pokrovsky & J. Schott 2000; E. H. Oelkers 2001; A. Steudel et al. 2017). Indeed, some of the secondary phyllosilicates found in soils on Earth and Mars are similar to those reported here, mixtures of serpentines and smectites. The high abundance of aluminum found in phyllosilicates produced from the OF series is in agreement with observations (N. Mangold et al. 2012; J. Carter et al. 2013, 2023). Aromatic molecules, such as benzoic acid, have already been identified in hydrothermal altered minerals on Mars, suggesting that they may represent a particularly abundant organic class on the planet (C. Freissinet et al. 2015; J. L. Eigenbrode et al. 2018; M. Millan et al. 2021, 2022; E. L. Scheller et al. 2022; A. Steele et al. 2022; S. Sharma et al. 2023).

Our results here suggest that abiotically sourced organic molecules may be a contributing factor to enhanced leaching of primary minerals and diversity of the secondary, in addition to other parameters like CO_2 (E. Dehouck et al. 2014; A. Gaudin et al. 2018). On Mars, the highly developed weathering sequences that have been found have been interpreted as paleosols but the climate in which they formed remains debated (e.g., J. Carter et al. 2015; M. Yu. Zolotov & M. V. Mironenko 2016; J. L. Bishop et al. 2020). Fluid organics may have promoted development of thick horizons of leached phases rich in Al/Si as well as sulfate precipitation, without the need for an enduring wet and warm climate. In an opposite scenario, it seems that higher pH, such as with benzylamine, inhibits leaching, especially of iron. The observed contradictory effects of organic molecules on the leaching of primary minerals needs to be better explored in the frame of understanding the climatic implications of weathering on early Mars and Earth. The chelating effect of organic salts that was observed here for Mg with Bz, is particularly relevant to Mars studies, where the lack of cation hosts are an outstanding problem (e.g., R. E. Milliken et al. 2009). Leached ions are typically sought out in sulfate or chloride salts, but organic salts may also constitute a reservoir for several ion species. That reservoir is likely minor at the geologic scale for the lack of ubiquitous organic matter at the surface of Mars, but could be nonnegligible at a local scale, richer in organic compounds.

In addition, as highlighted here, OM sequestration during hydrothermal alteration of primary minerals and formation of phyllosilicates is OM-phyllosilicate pairs dependent but seems highly favorable in a system where both phases are evolving

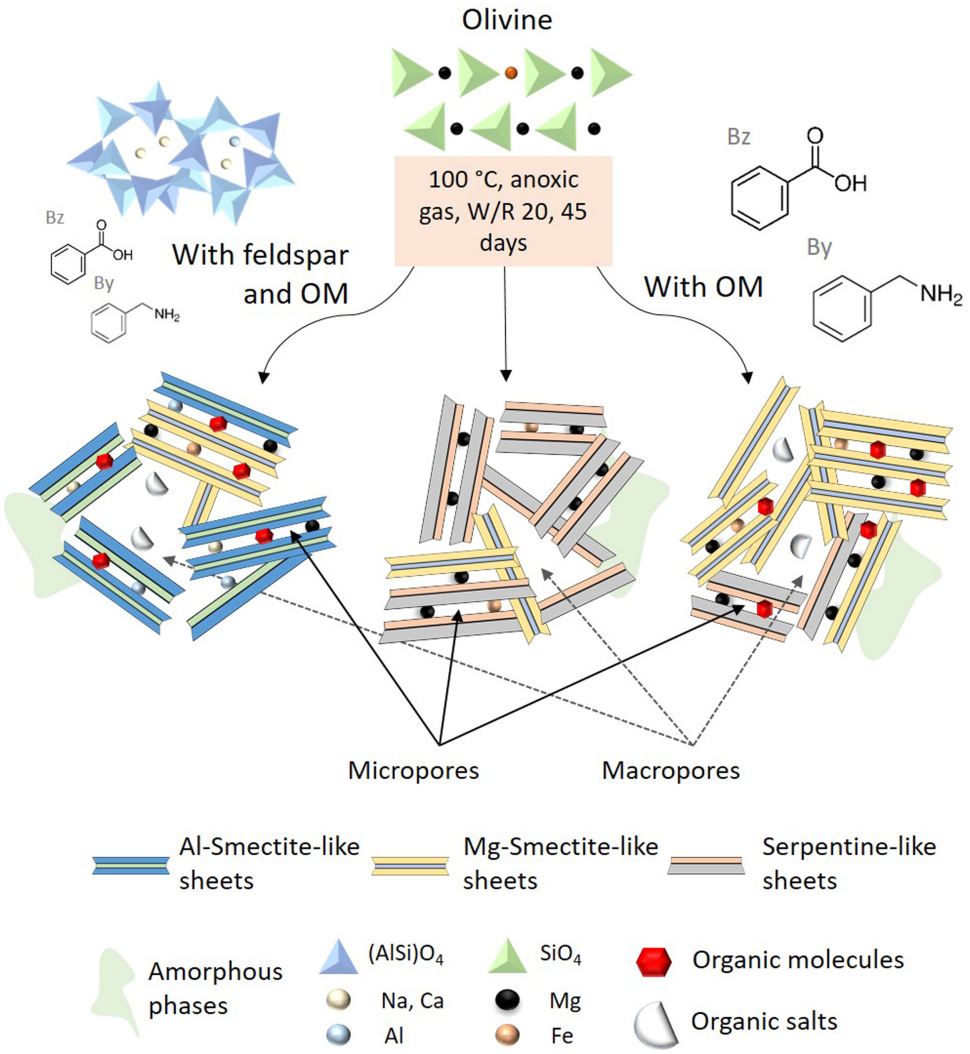

Figure 11. Illustration of the mineral evolution based on the results from our study with Mg-rich olivine, mixed with OM (benzyl molecules) and/or feldspar, under hydrothermal conditions at 100°C, in anoxic gas (Ar), with a water to rock (W/R) ratio of 20 and during 45 days. Without OM, results showed a majority of serpentine-like composition with high porosity whereas with benzoic acid (Bz) and/or benzylamine (By), more saponite-like compositions with lower porosity filled by OM were detected. When mixed with feldspar and OM, Al-smectite-like compositions are observed, also with OM in the pores.

together. Understanding why this is observed is paramount as it may guide current and future exploration of the other planetary surfaces, tailoring our search to the organic compounds that are more likely to have been adsorbed with the mineral phases (S. Sharma et al. 2023). Our nonwashed experimental samples can be considered to represent a geological scenario in which water has flowed away, leaving the mineral and allowing a high quantity of sorbed organic molecules to dry slowly. Additionally, the survivability of these molecules and salts, especially nitrogen compounds has to be tested under the space weathering conditions that are typical of Mars (O. Poch et al. 2015; R. dos Santos et al. 2016) or during thermal degradation over long periods of time (I. Criouet et al. 2023a) and with other minerals relevant to Mars (B. M. Tutolo & N. J. Tosca 2023). Nevertheless, a high adsorption (as evidenced here) may not be conducive to the analysis of these organic molecules by either spectroscopy or destructive chromatographic techniques, as they become entrapped within the minerals. Further investigations are required to ascertain the potential for the detection of organic matter in such evolved materials, as our analogs, following irradiations and analysis by spectroscopy or chromatographic techniques.

5. Conclusive Remarks

This study explored the influence of aromatic organic molecules on the secondary paragenesis of primary minerals commonly found in hydrothermal environments on planetary surfaces, such as early Mars, to produce relevant analogs of these conditions. Aromatic compounds functionalized with carboxylic acid (benzoic acid), amine (benzylamine), alkane (toluene), and an aliphatic alcohol were reacted with nonhydrated silicates (olivine and feldspar) under mild hydrothermal conditions. Over 45 days at 100°C, strong, irreversible interactions were observed between the organic and mineral phases, with organic molecules disrupting mineral dissolution by altering pH and forming chelates. This, in turn, affected phyllosilicate structuring. Nitrogen-bearing molecules and salts may also fill porous structures and interlayer spaces, delaying phase degradation.

The results suggest that high concentrations of abiotic organic molecules can significantly disrupt silicate paragenesis, while

facilitating organic adsorption onto minerals. These findings highlight the variability in organic-mineral interactions and the need for further studies across diverse systems, particularly in astrophysical contexts where organic matter is sought. Such production of analogs could then serve as a reference for spatial instrument calibrations and data comparison.

6. Declaration of Competing Interest

The authors declare that they have no known competing financial interests or personal relationships that could have appeared to influence the work reported in this paper.

Acknowledgments

We gratefully acknowledge support from the Agence Nationale de la Recherche (ANR 22-CE49-0007 ORGA-MISS—PI V. Vinogradoff) and the Program National de Planétologie (PNP) of CNRS/INSU France (PI V. Vinogradoff). V.V. thanks fruitful discussion with Sophie Nowak (Itodys, Université-CE Paris Diderot, UMR CNRS 7086) for XRD interpretations, Daniel Ferry (CINAM, Aix-marseille University, Marseille) for IR interpretation, Sandrine Bourrelly and Emily Bloch (Madirel, Aix-marseille Univserity) for their help with BET analysis and productive discussions, Vasile Heresanu (CINAM, Aix-Marseille Univesity) for his help with XRD analysis, and Gregory Excoffier (Spectropole of the *Fédération des Sciences Chimiques Marseille*, Aix Marseille University) for his help with elemental analysis.

Appendix
Supplementary Materials

This manuscript contains supplementary materials, such as Table A1 and Figures A1–A14 to support the work and main results: table of the compounds detected by GC-MS, chromatograms of the liquid fractions, infrared spectra of the dry aqueous fractions and solid phases, additional TEM and SEM images of the minerals, XRD data of the solid fractions including magnesium benzoate, and complementary N_2 sorption isotherms measured on the solid fractions.

Supplementary text for Section 2.1: detailed analytical protocol that is reported in Figure 1.

The pH was not buffered during the experiments, and measurements were conducted using universal indicator paper on the liquid fraction after separation from the solid fraction. It is important to note that the pH paper is subject to inherent inaccuracies, which necessitates the interpretation of the measurements as relative values rather than absolute.

The liquid fraction was separated into two aliquots (1.5 and 0.5 ml). Liquid–liquid extraction was done on the 0.5 ml water aliquot using 0.5 ml of dichloromethane (DCM) three times. The DCM fraction, which contained polar organic compounds and nonprotic soluble compounds, was reconcentrated to 0.5 ml and analyzed directly (without derivatization) with GC-MS (Figure 1). 200 μl of the water fraction (protic compounds) of these samples extracted with DCM was analyzed by ICP-MS (Figure 1), and the other 200 μl was slowly dried under nitrogen flux (N_2), in order to recover the precipitates (Figure 1).

The solid fractions were first dried in an oven at 60°C for one night before analysis. Samples containing carbon after this step (detected by EA) were systematically rewashed in order to retrieve the adsorbed carbon. A subfraction of 50 mg of this solid were first washed with 1.5 ml water (x2) and then 1.5 mL DCM (x2) to remove all nonadsorbed organic matter (Table 2). After washing, the solid is dried again in the oven (60°C, one night) and reanalyzed (Figure 1).

Table A1
Assignment of the Molecules Identified by GC-MS Analysis

N°	RT	Main Fragments m/z	Identified Molecules	Samples
1	4,53	59, 31	**Propanol**	All
2	4,74	91	**Toluene**	T+Pr By+T+Bz+Pr O+T+Pr O+By+T+Bz+Pr OF+T+Pr OF+By+T+Bz+Pr
3	6,13	56, 41, 31	**1-butanol***	All
4*	9,11		contamination	/
5	10,13	59	1-Butanol, 3-methoxy-	By+Pr T+Pr Bz+T+Pr By+T+Bz+Pr O+T+Pr
6	11,13	107 , 79	*unknown*	/
7	13,02	105,106,77	**Benzaldehyde**	All
8	14,04	106, 79, 91	**Benzylamine**	By+Pr By+T+Bz+Pr O+By+Pr O+By+T+Bz+Pr O+By/10+Pr/10 OF+By+Pr
9	14,35	103, 76, 50	**Benzonitrile**	By+Pr By+T+Bz+Pr

Table A1
(Continued)

N°	RT	Main Fragments m/z	Identified Molecules	Samples
				O+By+Pr
				O+By+T+Bz+Pr
				O+By/10+Pr/10
				OF+By+Pr
				OF+By+T+Bz+Pr
10	14,53	105, 136, 77	Benzoic acid, methyl ester	Bz+Pr
				By+T+Bz+Pr
				O+By+Pr
11	15,01	105, 120, 77	Acetophenone	By+T+Bz+Pr
				OF+By+T+Bz+Pr
12	16,49	123, 105, 77	N-propyl benzoate	Bz-Pr
				By+T+Bz+Pr
				O+Bz+Pr
				O+By+T+Bz+Pr
				OF+Bz+Pr
				OF+By+T+Bz+Pr
13	18,08	180,79,77	**Benzyl alcohol**	By+Pr
				By+T+Bz+Pr
				O+By+Pr
				O+By+T+Bz+Pr
				O+By/10+Pr/10
				All OF
14	19,71	108,79	Phenol 2-methyl	By+T+Bz+Pr
				OF+By+T+Bz+Pr
15	19,78	94, 66	**Phenol**	By+Pr
				Bz+Pr
				By+T+Bz+Pr
				O+By+Pr
				O+Bz+Pr
				O+By+T+Bz+Pr
				O+By/10+Pr/10
				All OF
16	19,94	145, 115, 146	2-Propenal, 2-methyl-3-phenyl-	By+T+Bz+Pr
				O+By+Pr
				O+By+T+Bz+Pr
				OF+Bz+Pr
				OF+By+T+Bz+Pr
17	20,75	108, 107, 77	Phenol-methyl	By+T+Bz+Pr
				O+By+T+Bz+Pr
				OF+By+T+Bz+Pr
18	20,85	108, 107, 77	Phenol-methyl	By+T+Bz+Pr
				O+By+T+Bz+Pr
				OF+By+T+Bz+Pr
19	21,26	91, 182	Bi-benzyl	By+T+Bz+Pr
20	22,69	168,169,167	$C_{12}H_{11}N$	By+T+Bz+Pr
21	22,91	183,182,168	$C_{12}H_{11}N$	By+T+Bz+Pr
22	23,05	121, 77, 91	Benzaldehyde oxime	By+Pr
				By+T+Bz+Pr
				O+By+Pr
				OF+By+Pr
23	24,46	182	*unknown*	By+T+Bz+Pr
24	24,93	105, 122, 77	**Benzoic acid**	Bz+Pr
				By+T+Bz+Pr
				O+Bz+Pr
				O+By+T+Bz+Pr
				OF+Bz+Pr
				OF+By+T+Bz+Pr
25	26,02	91, 106, 196	**Dibenzylamine**	By+Pr
				By+T+Bz+Pr
				O+By+Pr
				O+By+T+Bz+Pr
				O+By/10+Pr/10
				OF+By+Pr

Table A1
(Continued)

N°	RT	Main Fragments m/z	Identified Molecules	Samples
26	26,64	106, 149, 91	Acetamide, N-(phenylmethyl)	OF+By+T+Bz+Pr By+Pr By+T+Bz+Pr O+By+Pr O+By+T+Bz+Pr O+By/10+Pr/10 OF+By+Pr
27	27,17	91, 194, 195	**Benzylidenebenzylamine**	OF+By+T+Bz+Pr By+Pr By+T+Bz+Pr O+By+Pr O+By+T+Bz+Pr O+By/10+Pr/10 OF+By+Pr
28	27,96	135, 134, 79	**N-Benzylformamide**	OF+By+T+Bz+Pr By-Pr By+T+Bz+Pr O+By+T+Bz+Pr OF+By+Pr
29	28,08	105, 212, 77	Benzyl-benzoate	OF+By+T+Bz+Pr By+T+Bz+Pr
30	29,05	77, 105, 121	**Benzamide**	By+Pr By+T+Bz+Pr O+By+Pr O+By+T+Bz+Pr O+By/10+Pr/10 OF+By+Pr OF+By+T+Bz+Pr

Note. Numbers correspond to the one reported in Figures 2 (main text, and A1, A2, A3). Molecules in bold have been confirmed by standards compounds, other have been identified with the NIST database.

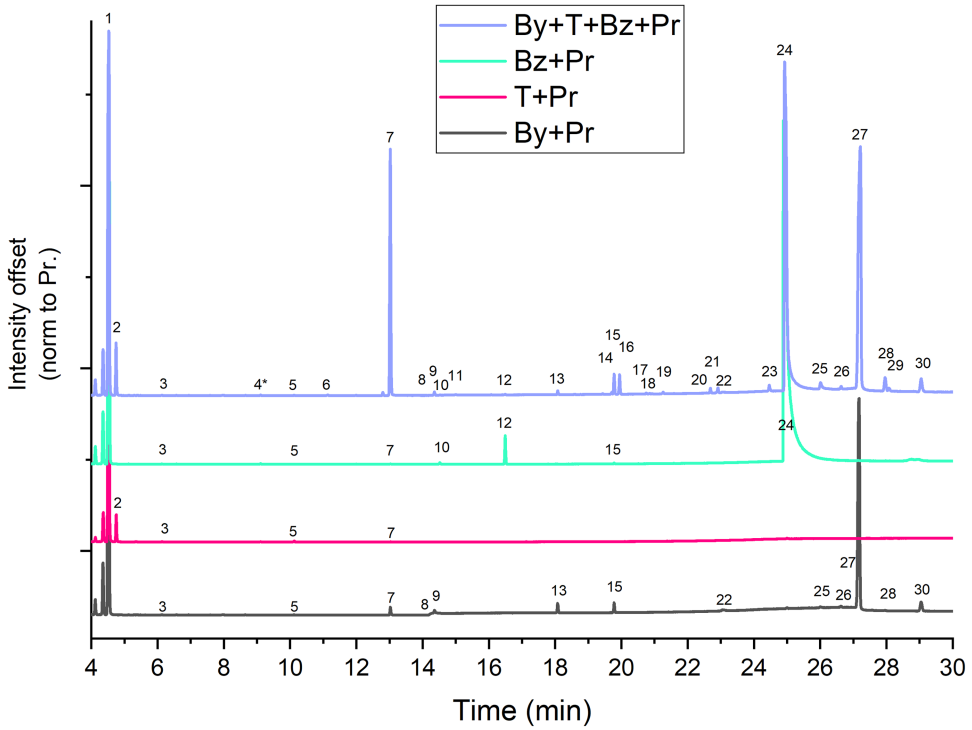

Figure A1. Chromatograms of liquid solutions (DCM fraction) from samples without minerals, By for Benzylamine, Bz for Benzoic acid, T for Toluene, and Pr for propanol. Intensity has been normalized to peak 1, propanol.

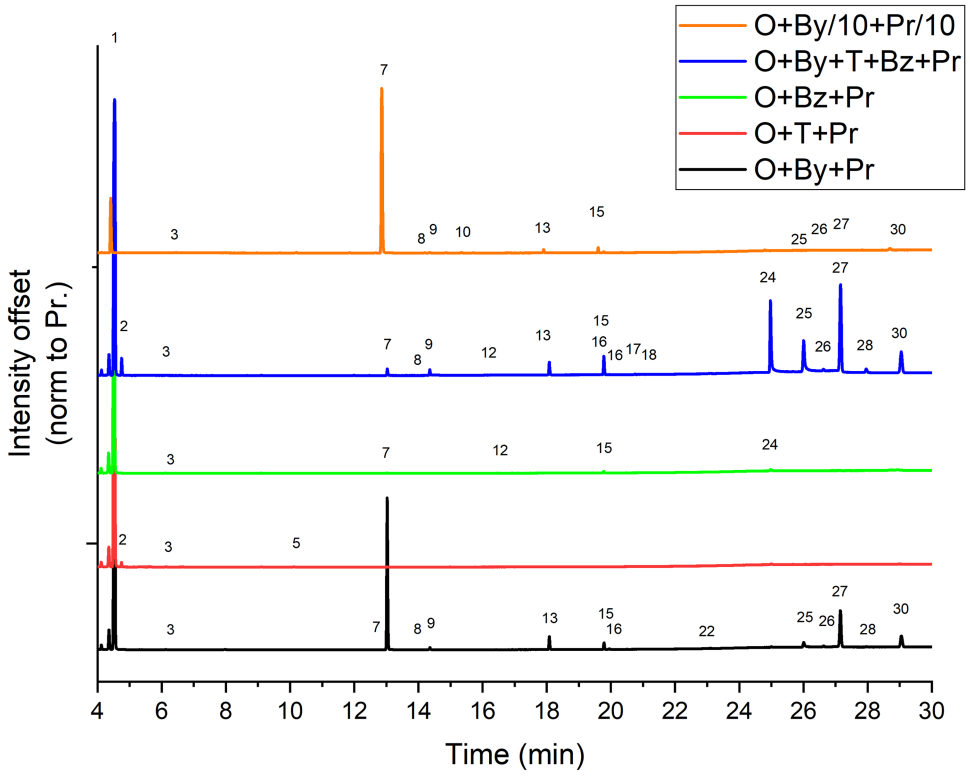

Figure A2. Chromatograms of liquid solutions (DCM fraction) from samples with the minerals, O for magnesium-rich olivine, By for Benzylamine, Bz for Benzoic acid, T for Toluene, and Pr for propanol. Intensity has been normalized to peak 1, propanol. Chromatogram from sample O+By/10+Pr/10 has been rescale to show peaks (x2). Numbers correspond to molecules assigned in table 4SI.

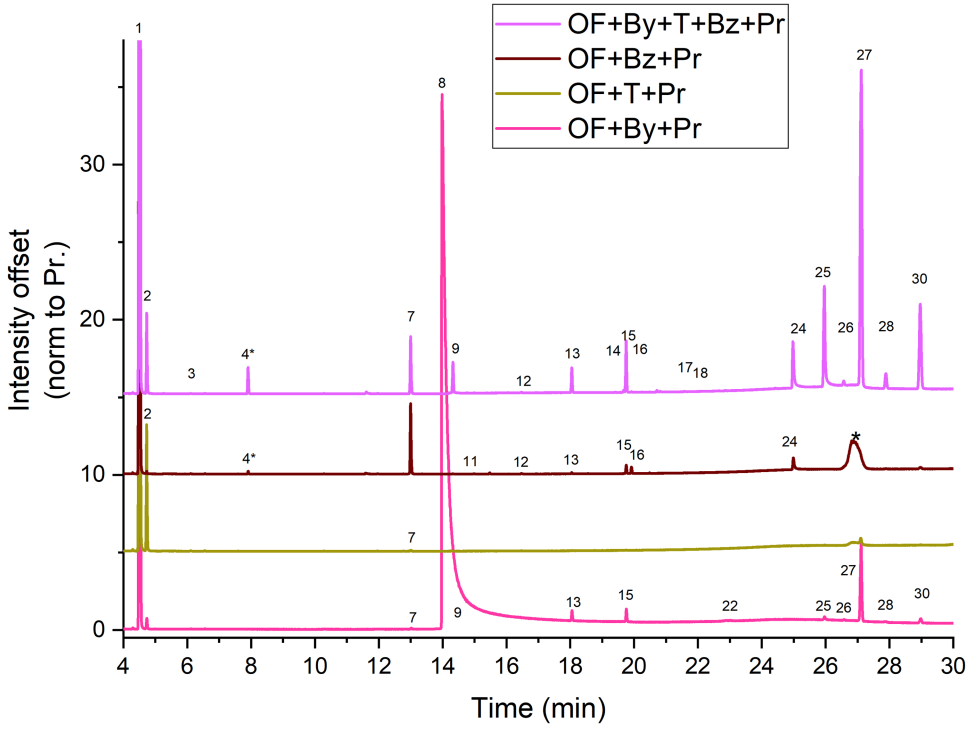

Figure A3. Chromatograms of liquid solutions (DCM fraction) from samples with the minerals, O for magnesium-rich olivine, F for sodium-rich feldspar, By for Benzylamine, Bz for Benzoic acid, T for Toluene, and Pr for propanol. Intensity has been normalized to peak 1, propanol. Numbers correspond to molecules assigned in Table 4SI.

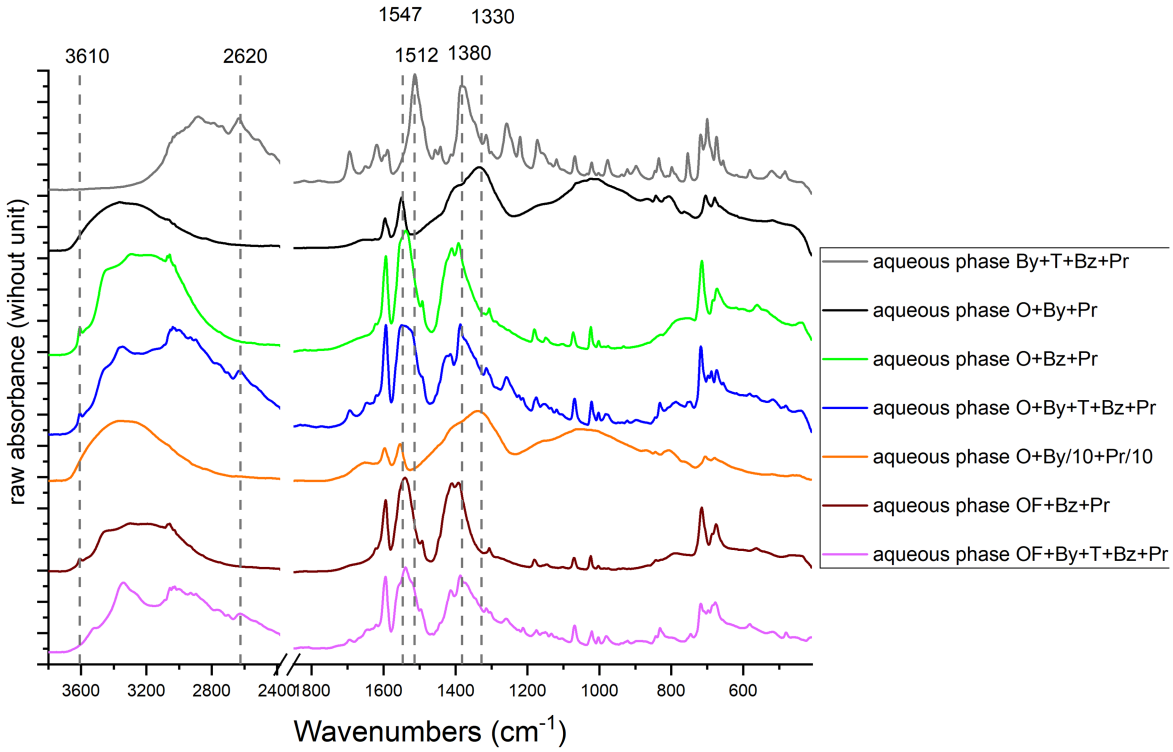

Figure A4. Infrared spectra of the dry aqueous phases of samples after hydrothermal alteration at 100°C. O for magnesium-rich olivine, F for feldspar, By for Benzylamine, Bz for Benzoic acid, T for Toluene, and Pr for propanol. We observed the existence of benzoate magnesium salt in samples with Bz (main bands highlighted by the dash lines–shown in Figure 3), and another salt in the sample with By, which has not been yet identified.

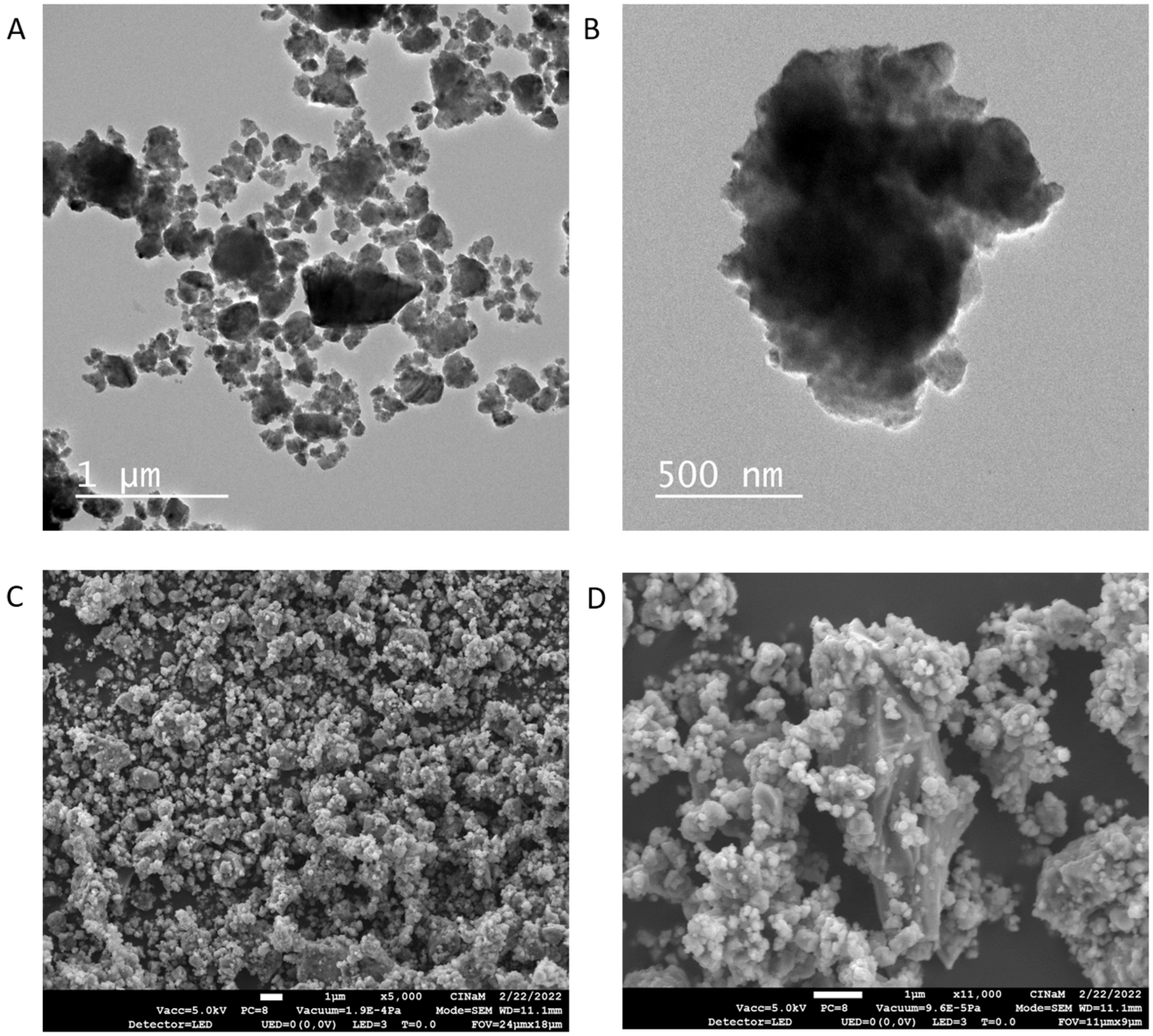

Figure A5. Images of Mg-rich olivine grains before reaction; the grain size of the olivine powder can be observed by TEM (A) and SEM (C) showing grains on average smaller than 10 μm. The texture of grain as observed by TEM (B) and SEM (D) shows a smooth and nonhydrated surface. The formula of our olivine (measured by EDX) was $Mg_{1.9}Fe_{0.1}SiO_4$.

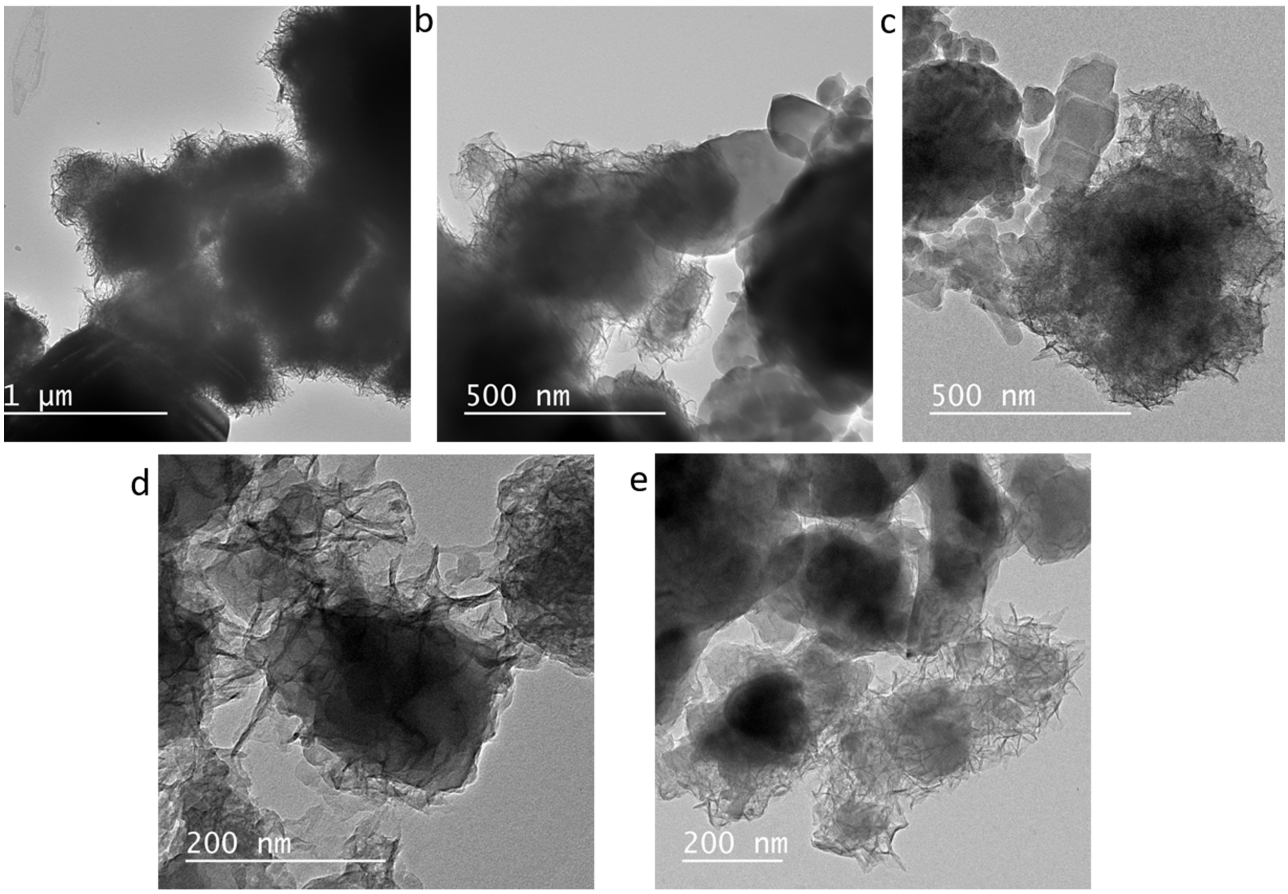

Figure A6. TEM images of the solid residues from experiments with Mg-rich olivine and Na-rich feldspar showing the identification of phyllosilicates agglomerate with almost unaltered grains of feldspar: from sample OF+By+Pr, (b) from sample OF+T+Pr, (c) from sample OF+Bz+Pr, (d) from samples OF+By+T+Bz+Pr, and (e) from sample OF w/o OM. O for magnesium-rich olivine, F for sodium-rich feldspar, By for Benzylamine, Bz for Benzylamine, T for Toluene, Pr for propanol, and OM for organic matter.

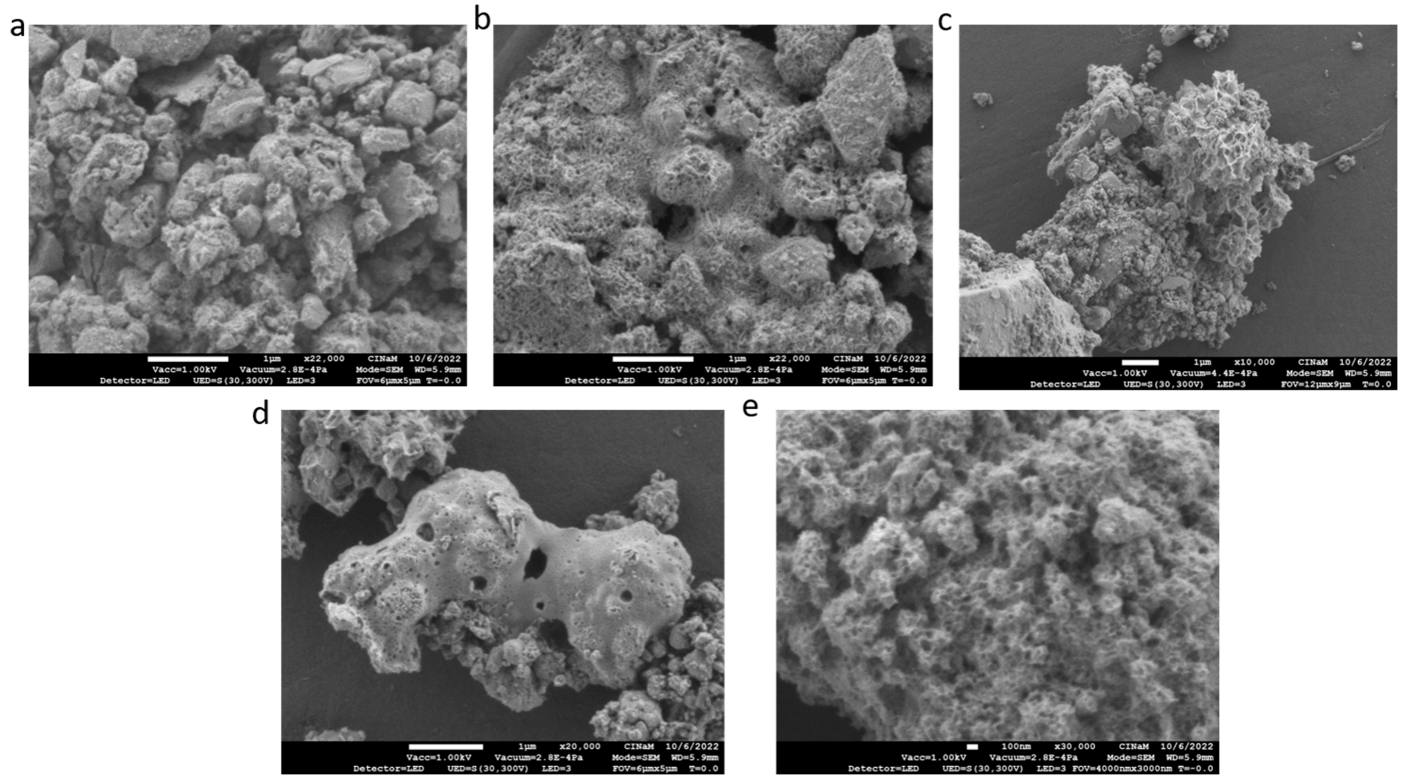

Figure A7. SEM images of the solid residues from experiments with magnesium-rich olivine and sodium-rich feldspar showing the structure of phyllosilicates agglomerated with feldspar grains covered by secondary minerals: from sample OF+By+Pr, (b) from sample OF+T+Pr, (c) from sample OF+Bz+Pr, (d) from samples OF+By+T+Bz+Pr, and (e) from sample OF w/o OM. O for magnesium-rich olivine, F for sodium-rich feldspar, By for Benzylamine, Bz for Benzylamine, T for Toluene, Pr for propanol, and OM for organic matter.

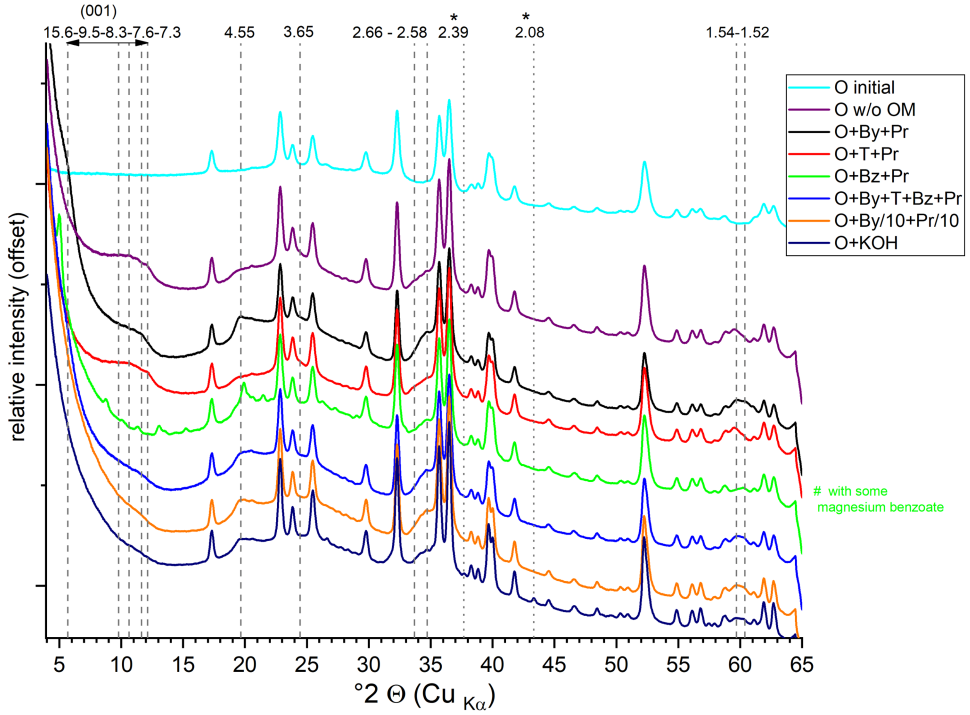

Figure A8. XRD pattern of the solid phases from the experiments with Mg-rich olivine (O) after hydrothermal alteration at 100°C with By for Benzylamine, Bz for Benzoic acid, T for Toluene, Pr for propanol, KOH for potassium hydroxide, and OM for organic matter. New diffraction lines are highlighted with their corresponding XRD lines in Å, which likely correspond to the presence of phyllosilicates. Also the increase of the baseline between 15° and 30°, and 30°–45° indicated the presence of amorphous phases. Additional lines in sample O+Bz+Pr are signatures from the magnesium benzoate cristal (Fig. S12), and additional lines in sample O+KOH (*) are likely correlated with a new phase with K. All the other lines belong to the olivine starting mineral.

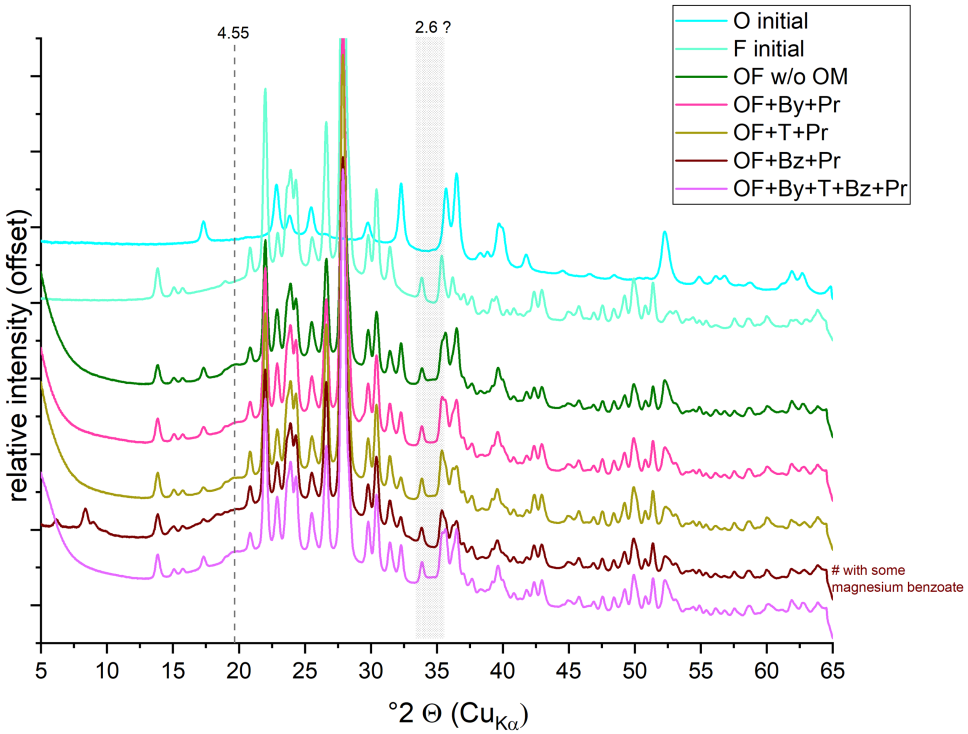

Figure A9. XRD pattern of the solid phases from the experiments with Mg-rich olivine (O) and Na-rich feldspar (F) after hydrothermal alteration at 100°C with By Benzylamine, Bz for Benzoic acid, T for Toluene, Pr for propanol, and OM for organic matter. New diffraction lines are difficult to observe, only one at 4.55 Å can be observed. We may suspect a broad line near 2.6 Å, but very small. Lines related to magnesium/sodium/calcium benzoate are also observed in sample OF +Bz+Pr.

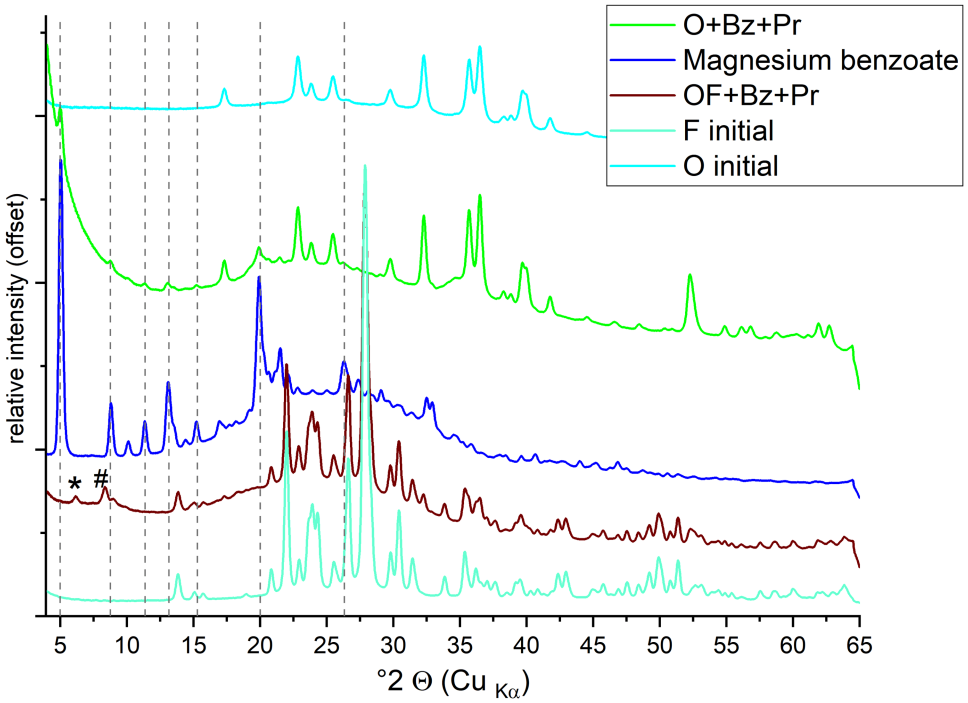

Figure A10. XRD pattern of magnesium benzoate standard compound compared to samples from O+Bz+Pr and OF+Bz+Pr. Lines from benzoate magnesium can be clearly identified in the diffractogram of the olivine solid residue, but not in the feldspar-rich residue (while the IR spectrum-Figure 3 was matching), which could indicate the presence of another counter ion of the benzoate, like sodium or calcium, indicated with the line labeled * on the diffractogram at ∼6°. The diffraction line noted # is likely pure crystal of benzoic acid (A. Terakita & S. R. Byrn, 2006; C. Butterhof et al. 2012).

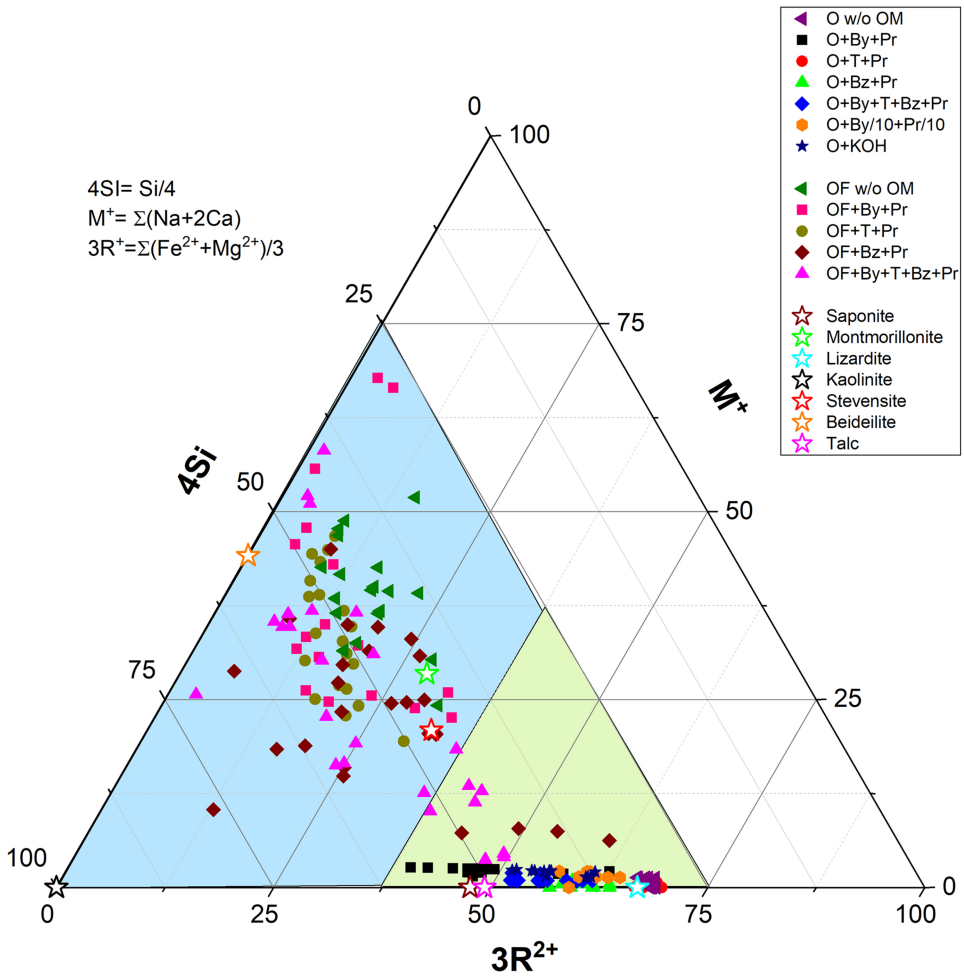

Figure A11. Ternary diagram (atomic %) showing the composition of phyllosilicates obtained by EDS analysis in the 4SI, M^{+}(Ca+Na), and $3R^{2+}$ (Fe+Mg) representation (A. Meunier & B. Velde 1989; A. Meunier 2005) for the solid fractions after 45 days of aqueous alteration at 100°C. O stands for magnesium-rich olivine, F for sodium-rich feldspar, By for Benzylamine, Bz for Benzylamine, T for Toluene, Pr for propanol, KOH for potassium hydroxide, and OM for organic matter. Two areas are shown below: the yellowish triangle for the olivine series and the blue triangle for the feldspar-olivine series. For each sample, at least 10 different locations were analyzed and are reported in the same label + color for the sample. Reference samples are indicated by stars in different colors, lizardite and talc taken from Ruff database, saponite from O. Grauby et al. (1994), high charge montmorillonite and beidellite from A. Meunier & B. Velde (1989), and stevensite and kaolinite from the webmineral database.

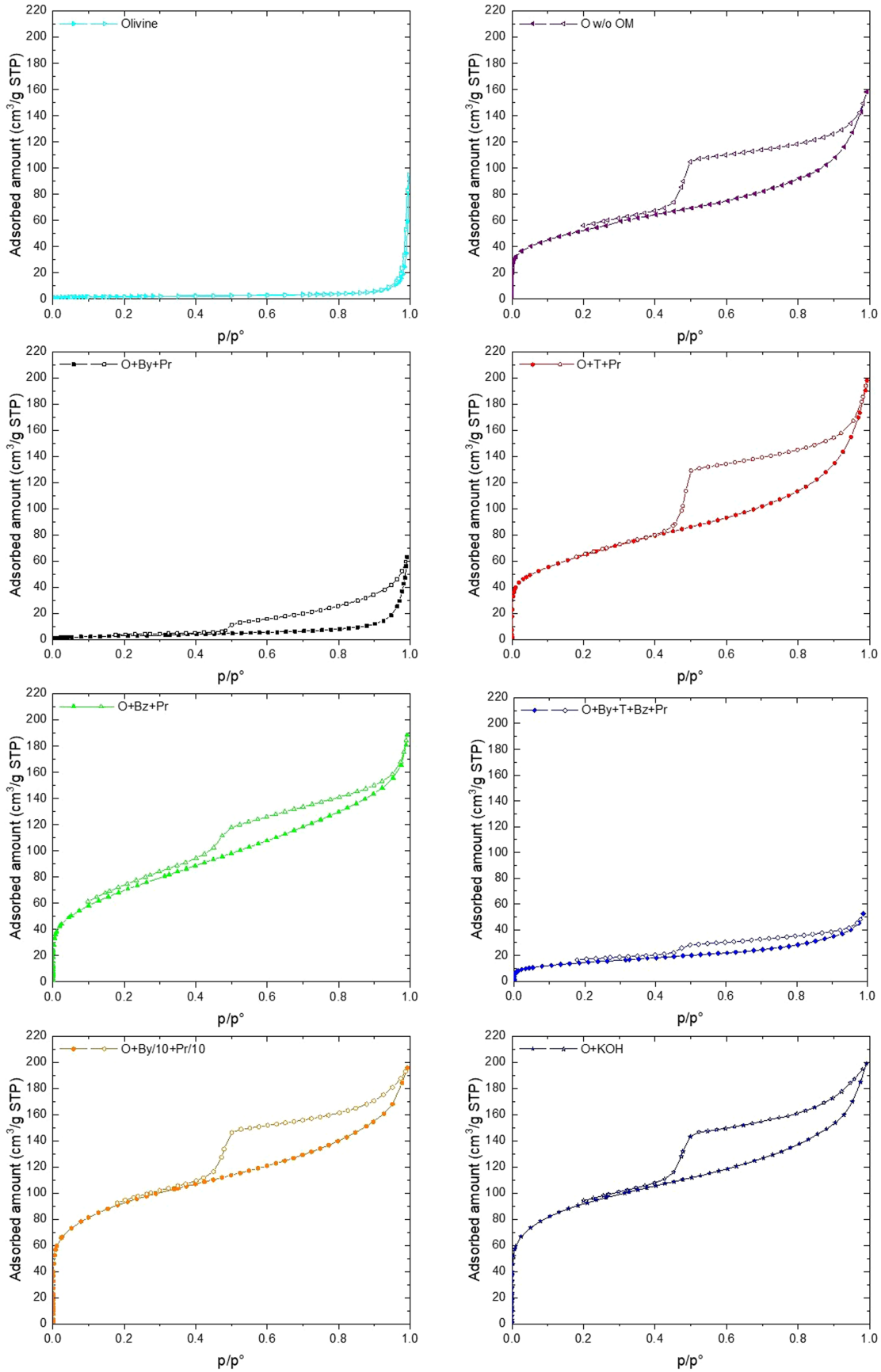

Figure A12. N_2 sorption isotherms measured at 77 K for the samples after 45 days of aqueous alteration at 100°C with Mg-rich olivine only. O stands for magnesium-rich olivine, organic molecules, By for Benzylamine, Bz for Benzoic acid, T for Toluene, Pr for Propanol, and KOH for potassium hydroxide.

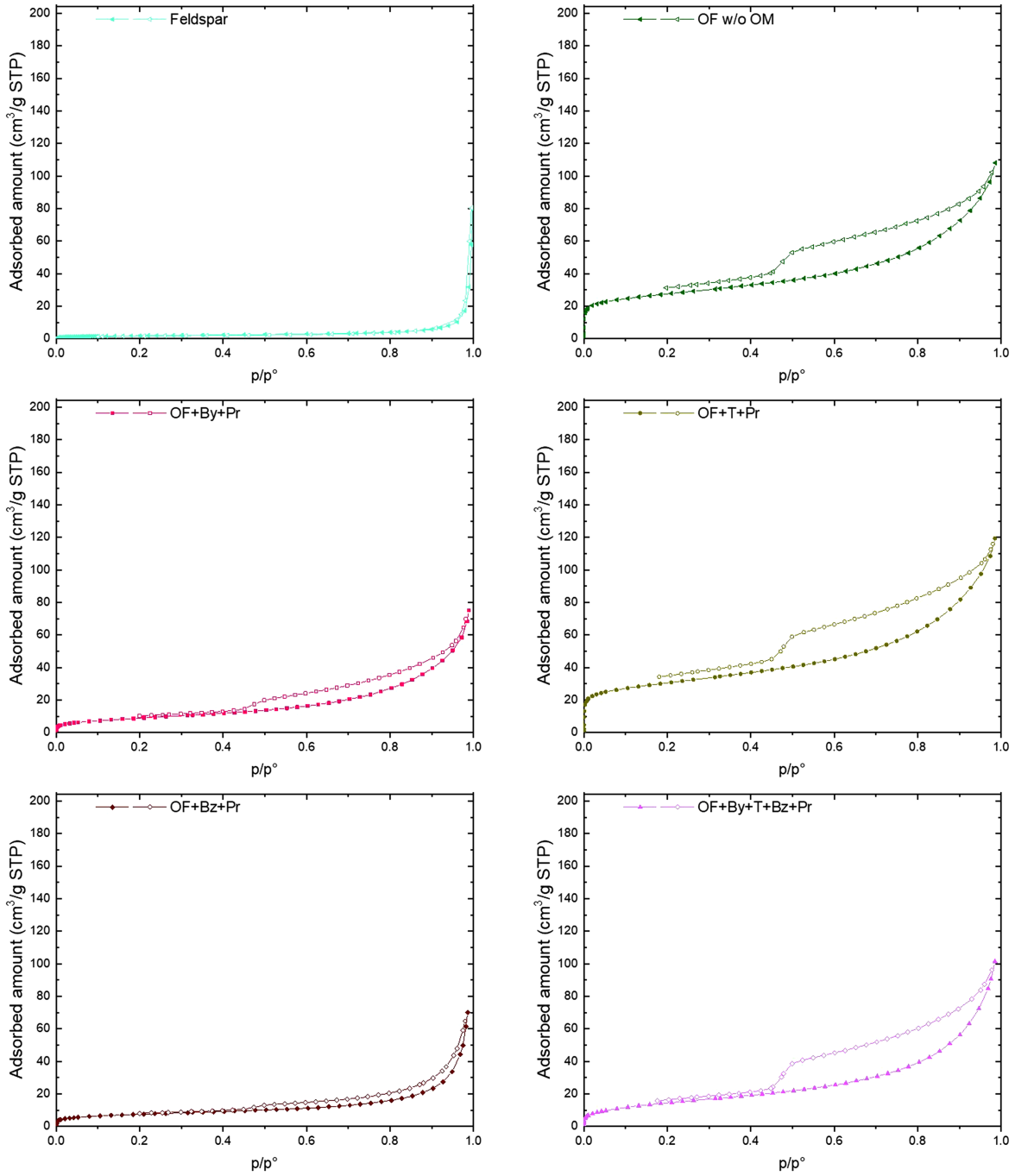

Figure A13. N2 sorption isotherms measured at 77 K for the samples after 45 days of aqueous alteration at 100°C with Mg-rich olivine and Na-rich feldspar. O stands for magnesium-rich olivine, F for Na-rich feldspar, By for Benzylamine, Bz for Benzoic acid, T for Toluene, and Pr for Propanol.

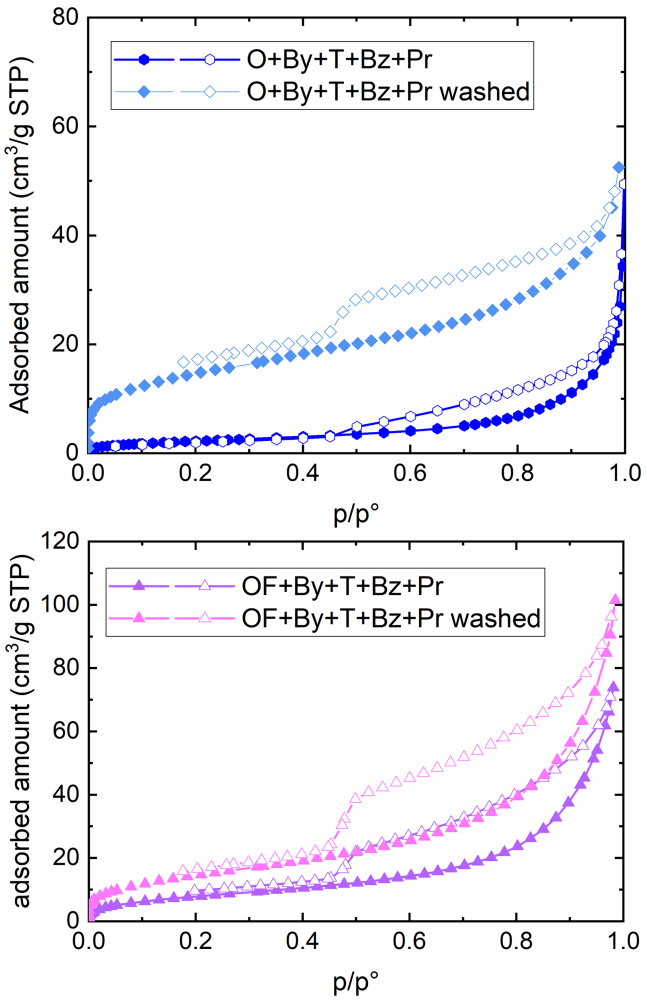

Figure A14. N2 sorption isotherms of the two samples showing differences before and after the washing procedure. The isotherm has changed with an increase of the step and porosity, as revealed by the shape. O stands for magnesium-rich olivine, F for Na-rich feldspar, By for Benzylamine, Bz for Benzoic acid, T for Toluene, and Pr for Propanol.

ORCID iDs

Vassilissa Vinogradoff https://orcid.org/0000-0003-4107-0980
Vincent Chevrier https://orcid.org/0000-0002-1111-587X

References

Alietti, A., & Mejsner, J. 1980, Structure of a Talc/Saponite Mixed-Layer Mineral, CCM, 28, 388
Aubrey, A. D., Cleaves, H. J., & Bada, J. L. 2009, The Role of Submarine Hydrothermal Systems in the Synthesis of Amino Acids, OLEB, 39, 91
Bailey, S. W. 1988, X-Ray Diffraction Identification of the Polytypes of Mica, Serpentine, and Chlorite, CCM, 36, 193
Berthonneau, J., Grauby, O., Ferrage, E., et al. 2014, Impact of Swelling Clays on the Spalling Decay of Building Limestones: Insights from X-Ray Diffraction Profile Modeling, EJMin, 26, 643
Bishop, J. L., Gross, C., Danielsen, J., Parente, M., Murchie, S. L., Horgan, B., Wray, J. J., Viviano, C., & Seelos, F. P. 2020, Multiple Mineral Horizons in Layered Outcrops at Mawrth Vallis, Mars, Signify Changing Geochemical Environments on Early Mars, Icarus, 341, 113634
Brearley, A. J. 1995, Aqueous Alteration and Brecciation in Bells, An Unusual, Saponite-Bearing, CM Chondrite, GeCoA, 59, 2291
Brucato, J. R., & Fornaro, T. 2019, Role of Mineral Surfaces in Prebiotic Processes and Space-Like Conditions, in Biosignatures for Astrobiology, Advances in Astrobiology and Biogeophysics, ed. B. Cavalazzi & F. Westall (Cham: Springer), 183
Butterhof, C., Milius, W., & Breu, J. 2012, Co-Crystallisation of Benzoic Acid with Sodium Benzoate: the Significance of Stoichiometry, CEG, 14, 3945
Carter, J., Loizeau, D., Mangold, N., Poulet, F., & Bibring, J.-P. 2015, Widespread Surface Weathering on Early Mars: a Case for a Warmer and Wetter Climate, Icarus, 248, 373
Carter, J., Poulet, F., Bibring, J.-P., Mangold, N., & Murchie, S. 2013, Hydrous Minerals on Mars as seen by the CRISM and OMEGA Imaging Spectrometers: Updated Global View, JGRE, 118, 831
Carter, J., Riu, L., Poulet, F., et al. 2023, A Mars Orbital Catalog of Aqueous Alteration Signatures (MOCAAS), Icar, 389, 115164
Castillo-Rogez, J. C., Neveu, M., McSween, H. Y., et al. 2018, Insights into Ceres's Evolution from Surface Composition, M&PS, 53, 1820
Cecilia, J. A., García-Sancho, C., Vilarrasa-García, E., Jiménez-Jiménez, J., & Rodriguez-Castellón, E. 2018, Synthesis, Characterization, Uses and Applications of Porous Clays Heterostructures: A Review, Chem. Rec., 18, 1085
Chae, H. J., Nam, I.-S., Ham, S. W., & Hong, S. B. 2001, Physicochemical Characteristics of Pillared Interlayered Clays, Catal. Today, Nanomaterials in Catalysis, 68, 31
Chan, M. A., Hinman, N. W., Potter-McIntyre, S. L., et al. 2019, Deciphering Biosignatures in Planetary Contexts, AsBio, 19, 1075
Cleaves, H. J., II, Scott, A. M., Hill, F. C., et al. 2012, Mineral–Organic Interfacial Processes: Potential Roles in the Origins of Life, CSRev, 41, 5502
Cliff, G., & Lorimer, G. W. 1975, The Quantitative Analysis of Thin Specimens, JMic, 103, 203
Colín-García, M., Heredia, A., Cordero, G., et al. 2016, Hydrothermal Vents and Prebiotic Chemistry: A Review, BoSGM, 68, 599
Criouet, I., Viennet, J.-C., Balan, E., et al. 2023a, Experimental Investigations of the Preservation/Degradation of Microbial Signatures in the Presence of Clay Minerals Under Martian Subsurface Conditions, Icar, 406, 115743
Criouet, I., Viennet, J. C., Baron, F., et al. 2023b, Influence of pH on the Hydrothermal Synthesis of Al-Substituted Smectites (Saponite, Beidellite, and Nontronite), CCM, 71, 539
Daval, D., Sissmann, O., Menguy, N., et al. 2011, Influence of Amorphous Silica Layer Formation on the Dissolution Rate of Olivine at 90°C and Elevated pCO2, ChGeo, 284, 193
de Jong, T. J., Demertzi, A. D., Robinson, W. E., & Huck, W. T. S. 2025, Environmental History is Transferred via Minerals Altering Formose Reaction Pathways, AngCh, n/a, e202504659
Deer, W. A., Howie, R. A., & Zussman, J. 2013, An Introduction to the Rock-Forming Minerals (London: Mineralogical Society of Great Britain and Ireland)
Dehouck, E., Gaudin, A., Mangold, N., et al. 2014, Weathering of Olivine under CO_2 Atmosphere: A Martian Perspective, GeCoA, 135, 170
dos Santos, R., Patel, M., Cuadros, J., & Martins, Z. 2016, Influence of Mineralogy on the Preservation of Amino Acids under Simulated Mars Conditions, Icar, 277, 342
Drever, J. I., & Stillings, L. L. 1997, The Role of Organic Acids in Mineral Weathering, Colloids Surf. Physicochem. Eng. Asp., Aquatic Colloid and Surface Chemistry, 120, 167
Drits, V. A. 1997, Mixed-Layer Minerals, in Modular Aspects of Minerals, ed. S. Merlino (Paris: European Mineralogical Union)
Eigenbrode, J. L., Summons, R. E., Steele, A., et al. 2018, Organic Matter Preserved in 3 Billion-year-Old Mudstones at Gale Crater, Mars, Sci, 360, 1096
Ertem, G., Ertem, M. C., McKay, C. P., & Hazen, R. M. 2017, Shielding Biomolecules from Effects of Radiation by Mars Analog Minerals and Soils, IJAsB, 16, 280
Evans, B. W. 2004, The Serpentinite Multisystem Revisited: Chrysotile Is Metastable, IGRv, 46, 479
Feuillie, C., Daniel, I., Michot, L. J., & Pedreira-Segade, U. 2013, Adsorption of Nucleotides onto Fe–Mg–Al Rich Swelling Clays, GeCoA, 120, 97
Foucher, F., Hickman-Lewis, K., Hutzler, A., et al. 2021, Definition and use of Functional Analogues in Planetary Exploration, P&SS, 197, 105162
Freissinet, C., Glavin, D. P., Mahaffy, P. R., et al. 2015, Organic Molecules in the Sheepbed Mudstone, Gale Crater, Mars, JGRE, 120, 495
Fritsch, E., Balan, E., Petit, S., & Juillot, F. 2021, Structural, Textural, and Chemical Controls on the OH Stretching Vibrations in Serpentine-Group Minerals, EJMin, 33, 447
Ganor, J., Reznik, I. J., & Rosenberg, Y. O. 2009, Organics in Water-Rock Interactions, RvMG, 70, 259
Gaudin, A., Dehouck, E., Grauby, O., & Mangold, N. 2018, Formation of Clay Minerals on Mars: Insights from Long-term Experimental Weathering of Olivine, Icar, 311, 210

Gaudin, A., Dehouck, E., & Mangold, N. 2011, Evidence for Weathering on Early Mars from a Comparison with Terrestrial Weathering Profiles, Icar, 216, 257
Golubev, S. V., Bauer, A., & Pokrovsky, O. S. 2006, Effect of pH and Organic Ligands on the Kinetics of Smectite Dissolution at 25°C, GeCoA, 70, 4436
Grauby, O., Petit, S., Decarreau, A., & Baronnet, A. 1994, EJMin, 6, 99
Gudbrandsson, S., Wolff-Boenisch, D., Gislason, S. R., & Oelkers, E. H. 2014, Experimental Determination of Plagioclase Dissolution Rates as a Function of its Composition and pH at 22°C, GeCoA, 139, 154
Hausrath, E. M., Treiman, A. H., Vicenzi, E., et al. 2008, Short- and Long-Term Olivine Weathering in Svalbard: Implications for Mars, AsBio, 8, 1079
Hemingway, J. D., Rothman, D. H., Grant, K. E., et al. 2019, Mineral Protection Regulates Long-Term Global Preservation of Natural Organic Carbon, Natur, 570, 228
Heřmanská, M., Voigt, M. J., Marieni, C., Declercq, J., & Oelkers, E. H. 2022, A Comprehensive and Internally Consistent Mineral Dissolution Rate Database: Part I: Primary Silicate Minerals and Glasses, ChGeo, 597, 120807
Isono, Y., Tachibana, S., Naraoka, H., et al. 2019, Bulk Chemical Characteristics of Soluble Polar Organic Molecules Formed Through Condensation of Formaldehyde: Comparison with Soluble Organic Molecules in Murchison Meteorite, GeocJ, 53, 41
Jacquemot, P., Viennet, J.-C., Bernard, S., et al. 2019, The Degradation of Organic Compounds Impacts the Crystallization of Clay Minerals and Vice Versa, NatSR, 9, 20251
Janecky, D. R., & Seyfried, W. E. 1986, Hydrothermal Serpentinization of Peridotite within the Oceanic Crust: Experimental Investigations of Mineralogy and Major Element Chemistry, GeCoA, 50, 1357
Johnson, N. C., Thomas, B., Maher, K., et al. 2014, Olivine Dissolution and Carbonation Under Conditions Relevant for In Situ Carbon Storage, ChGeo, 373, 93
Kebukawa, Y., Kobayashi, H., Urayama, N., et al. 2019, Nanoscale Infrared Imaging Analysis of Carbonaceous Chondrites to Understand Organic-Mineral Interactions During Aqueous Alteration, PNAS, 116, 753
Kleber, M., Bourg, I. C., Coward, E. K., et al. 2021, Dynamic Interactions at the Mineral–Organic Matter Interface, NRvEE, 2, 402
Kleber, M., Eusterhues, K., Keiluweit, M., et al. 2015, Chapter One–Mineral–Organic Associations: Formation, Properties, and Relevance in Soil Environments, in Advances in Agronomy, ed. D. L. Sparks (New York: Academic), 1
Kloprogge, J. T., & Ponce, C. P. 2021, Spectroscopic Studies of Synthetic and Natural Saponites: A Review, Mine, 11, 112
Kooli, F., & Jones, W. 1997, Characterization and Catalytic Properties of a Saponite Clay Modified by Acid Activation, ClMin, 32, 633
Lagache, M. 1976, New Data on the Kinetics of the Dissolution of Alkali Feldspars at 200°C in CO_2 Charged Water, GeCoA, 40, 157
Lagaly, G., Ogawa, M., & Dékány, I. 2013, Chapter 10.3—Clay Mineral–Organic Interactions, in Developments in Clay Science, Handbook of Clay Science, ed. F. Bergaya & G. Lagaly (Amsterdam: Elsevier), 435
Lambert, J.-F. 2008, Adsorption and Polymerization of Amino Acids on Mineral Surfaces: A Review, OLEB, 38, 211
Le Guillou, C., Bernard, S., Brearley, A. J., & Remusat, L. 2014, Evolution of Organic Matter in Orgueil, Murchison and Renazzo During Parent Body Aqueous Alteration: In Situ Investigations, GeCoA, 131, 368
Lee, C., Weber, J. M., Rodriguez, L. E., et al. 2022, Chirality in Organic and Mineral Systems: A Review of Reactivity and Alteration Processes Relevant to Prebiotic Chemistry and Life Detection Missions, Symm, 14, 460
Madejová, J., Gates, W. P., & Petit, S. 2017, Chapter 5—IR Spectra of Clay Minerals, in Developments in Clay Science, Infrared and Raman Spectroscopies of Clay Minerals, ed. W. P. Gates et al. (Amsterdam: Elsevier), 107
Mangold, N., Carter, J., Poulet, F., et al. 2012, Late Hesperian Aqueous Alteration at Majuro crater, Mars, P&SS, 72, 18
Marlow, J. J., Martins, Z., & Sephton, M. A. 2011, Organic Host Analogues and the Search for Life on Mars, IJAsB, 10, 31
Mayer, L. M. 1994, Relationships Between Mineral Surfaces and Organic Carbon Concentrations in Soils and Sediments, ChGeo, 114, 347
McMahon, S., & Cosmidis, J. 2022, False Biosignatures on Mars: Anticipating Ambiguity, J. Geol. Soc., 179, jgs2021-050
Ménez, B., Pisapia, C., Andreani, M., et al. 2018, Abiotic Synthesis of Amino Acids in the Recesses of the Oceanic Lithosphere, Natur, 564, 59
2005, Crystal Chemistry of Clay Minerals, in Clays, Meunier, A. (ed.) (Berlin: Springer), 61
Meunier, A., & Velde, B. 1989, Solid Solutions in I/S Mixed-Layer Minerals and Illite, AmMin., 74, 1106
Michalski, J. R., Dobrea, E. Z. N., Niles, P. B., & Cuadros, J. 2017, Ancient Hydrothermal Seafloor Deposits in Eridania Basin on Mars, NatCo, 8, 15978
Michot, L. J., & Villiéras, F. 2013, Chapter 2.10—Surface Area and Porosity, in Developments in Clay Science, Handbook of Clay Science, ed. F. Bergaya & G. Lagaly (Amsterdam: Elsevier), 319
Millan, M., Teinturier, S., Malespin, C. A., et al. 2021, Organic Molecules Revealed in Mars's Bagnold Dunes by Curiosity's Derivatization Experiment, NatAs, 6, 129
Millan, M., Williams, A. J., McAdam, A. C., et al. 2022, Sedimentary Organics in Glen Torridon, Gale Crater, Mars: Results from the SAM Instrument Suite and Supporting Laboratory Analyses, JGRE, 127, e2021JE007107
Milliken, R. E., Fischer, W. W., & Hurowitz, J. A. 2009, Missing Salts on Early Mars, GeoRL, 36, L11202
Muchowska, K. B., Varma, S. J., & Moran, J. 2019, Synthesis and Breakdown of Universal Metabolic Precursors Promoted by Iron, Natur, 569, 104
Neubeck, A., Duc, N. T., Bastviken, D., Crill, P., & Holm, N. G. 2011, Formation of H2 and CH4by Weathering of Olivine at Temperatures between 30 and 70°C, GeoTr, 12, 6
Neubeck, A., Duc, N. T., Hellevang, H., et al. 2014, Olivine Alteration and H2 Production in Carbonate-Rich, Low Temperature Aqueous Environments, P&SS, 96, 51
Oelkers, E. H. 2001, An Experimental Study of Forsterite Dissolution Rates as a Function of Temperature and Aqueous Mg and Si Concentrations, ChGeo, 175, 485
Oelkers, E. H., Declercq, J., Saldi, G. D., Gislason, S. R., & Schott, J. 2018, Olivine Dissolution Rates: A Critical Review, ChGeo, 500, 1
Oyanagi, R., Okamoto, A., & Tsuchiya, N. 2017, Mechanisms of Serpentinization Utilizing Olivine–Plagioclase–H_2O System under Hydrothermal Conditions, PrEPS, 17, 686
Pedreira-Segade, U., Feuillie, C., Pelletier, M., Michot, L. J., & Daniel, I. 2016, Adsorption of Nucleotides onto Ferromagnesian Phyllosilicates: Significance for the Origin of Life, GeCoA, 176, 81
Peters, S., Semenov, D. A., Hochleitner, R., & Trapp, O. 2023, Synthesis of Prebiotic Organics from CO_2 by Catalysis with Meteoritic and Volcanic Particles, NatSR, 13, 6843
Poch, O., Jaber, M., Stalport, F., et al. 2015, Effect of Nontronite Smectite Clay on the Chemical Evolution of Several Organic Molecules under Simulated Martian Surface Ultraviolet Radiation Conditions, AsBio, 15, 221
Pokrovsky, O. S., & Schott, J. 2000, Kinetics and Mechanism of Forsterite Dissolution at 25°C and pH from 1 to 12, GeCoA, 64, 3313
Riu, L., Poulet, F., Bibring, J.-P., & Gondet, B. 2019, The M3 Project: 2—Global Distributions of Mafic Mineral Abundances on Mars, Icar, 322, 31
Rouquerol, J., Rouquerol, F., Llewellyn, P., Maurin, G., & Sing, K. 2013, Adsorption by Powders and Porous Solids: Principles, Methodology and Applications (New York: Academic)
Scheller, E. L., Razzell Hollis, J., Cardarelli, E. L., et al. 2022, Aqueous Alteration Processes in Jezero Crater, Mars—Implications for Organic Geochemistry, Sci, 378, 1105
Schoonen, M., Smirnov, A., & Cohn, C. 2004, A Perspective on the Role of Minerals in Prebiotic Synthesis, Ambio, 33, 539
Serra, C., Grauby, O., Ferry, D., et al. 2025, Experimental Investigations of Mineral-Organic Chondritic Analogs Under Hydrothermal Conditions: Implications for Carbonaceous Asteroids, GeCoA, 398, 29
Serra, C., Vinogradoff, V., Danger, G., Coulet, M.-V., & Duvernay, F. 2024, Unexpected Mineral Impact on Organic Evolution During Simulated Aqueous Alteration in Asteroids, Icar, 423, 116273
Sharma, S., Roppel, R. D., Murphy, A. E., et al. 2023, Diverse Organic-mineral Associations in Jezero Crater, Mars, Natur, 619, 724
Steele, A., Benning, L. G., Wirth, R., et al. 2022, Organic Synthesis Associated with Serpentinization and Carbonation on Early Mars, Sci, 375, 172
Steudel, A., Friedrich, F., Schuhmann, R., et al. 2017, Characterization of a Fine-Grained Interstratification of Turbostratic Talc and Saponite, Mine, 7, 5
Teece, B. L., Havig, J. R., Hamilton, T. L., & Barge, L. M. 2024, Geochemical Context for Hydrothermal Organic Molecules in Mars-Analog Samples from Earth, NatAs, 8, 1513
Terakita, A., & Byrn, S. R. 2006, Structure and Physical Stability of Hydrates and Thermotropic Mesophase of Calcium Benzoate, JPhmS, 95, 1162
Thommes, M., Kaneko, K., Neimark, A. V., et al. 2015, Physisorption of Gases, with Special Reference to the Evaluation of Surface Area and Pore Size Distribution (IUPAC Technical Report), Pure Appl. Chem., 87, 1051

Tomeoka, K., & Buseck, P. R. 1988, Matrix Mineralogy of the Orgueil CI Carbonaceous Chondrite, GeCoA, 52, 1627
Tutolo, B. M., & Tosca, N. J. 2023, Observational Constraints on the Process and Products of Martian Serpentinization, SciA, 9, eadd8472
Velde, B. B., & Meunier, A. 2008, The Origin of Clay Minerals in Soils and Weathered Rocks (Berlin: Springer)
Veniale, F., & Van der Marel, H. W. 1968, A Regular Talc-Saponite Mixed-Layer Mineral from Ferriere, Nure Valley (Piacenza Province, Italy), CoMP, 17, 237
Viennet, J.-C., Bernard, S., Le Guillou, C., et al. 2019, Experimental Clues for Detecting Biosignatures on Mars, Geochemical Perspectives Letters, 12, 28, 10.7185/geochemlet.1931
Viennet, J.-C., Le Guillou, C., Remusat, L., et al. 2022, Experimental Investigation of Fe-clay/Organic Interactions Under Asteroidal Conditions, GeCoA, 318, 352
Vinogradoff, V., Bernard, S., Le Guillou, C., & Remusat, L. 2018, Evolution of Interstellar Organic Compounds Under Asteroidal Hydrothermal Conditions, Icar, 305, 358
Vinogradoff, V., Le Guillou, C., Bernard, S., et al. 2020, Influence of Phyllosilicates on the Hydrothermal Alteration of Organic Matter in Asteroids: Experimental Perspectives, GeCoA, 269, 150
Vinogradoff, V., Leyva, V., Mates-Torres, E., et al. 2024, Olivine-Catalyzed Glycolaldehyde and Sugar Synthesis Under Aqueous Conditions: Application to Prebiotic Chemistry, E&PSL, 626, 118558
Welch, S. A., & Ullman, W. J. 1993, The Effect of Organic Acids on Plagioclase Dissolution Rates and Stoichiometry, GeCoA, 57, 2725
Wogelius, R. A., & Walther, J. V. 1991, Olivine Dissolution at 25°C: Effects of pH, CO2, and Organic Acids, GeCoA, 55, 943
Xu, H., Liu, Q., Jin, Z., et al. 2024, Organic Compounds in Geological Hydrothermal Systems: A Critical Review of Molecular Transformation and Distribution, ESRv, 252, 104757
Zolotov, M. Yu., & Mironenko, M. V. 2016, Chemical Models for Martian Weathering Profiles: Insights into Formation of Layered Phyllosilicate and Sulfate Deposits, Icarus, 275, 203